

Optical constants of carbon dioxide ice

Stephen G. Warren

Laboratory measurements of the absorption coefficient and refractive index of solid CO₂ are reviewed for all parts of the electromagnetic spectrum from the ultraviolet to the microwave with emphasis on values for temperatures above 77 K. The available measurements in some cases require reinterpretation. A compilation of the spectral absorption coefficient k_{abs} is made for 52-nm to 160-nm wavelength (with some gaps because of lack of data), and the complex refractive index is then computed by Kramers-Kronig analysis. The uncertainty in imaginary refractive index is discussed; it varies greatly with wavelength. The real part of the refractive index is close to 1.4 for all parts of the spectrum except near strong absorption bands and is accurate to ± 0.05 outside those bands. No measurements of absorption are available for 180–330-nm, 1.0–2.5- μm , and 25- μm –25-mm wavelength, except in the strong narrow absorption lines. Remeasurement of k_{abs} is also needed for parts of the IR spectrum between 2.5 and 25 μm because of experimental error in the available measurements.

I. Introduction

Understanding the reflection, transmission, absorption, and emission of radiation by materials containing CO₂ ice requires knowledge of the optical constants of pure clear solid CO₂ as functions of wavelength: the absorption coefficient k_{abs} (units of inverse length) and the refractive index m_{Re} . They are combined as real and imaginary parts of the complex index of refraction $m(\lambda) = m_{\text{Re}}(\lambda) - im_{\text{Im}}(\lambda)$, where λ is the wavelength in vacuum and $k_{\text{abs}} = 4\pi m_{\text{Im}}/\lambda$. The propagation of an electromagnetic wave in CO₂-ice is described by $m(\lambda)$ or by the complex relative permittivity, $\epsilon(\lambda) = \epsilon_{\text{Re}}(\lambda) - i\epsilon_{\text{Im}}(\lambda)$, where $m^2 = \epsilon$. ϵ_{Re} is often called the dielectric constant.

This review is directed toward planetary science applications, so emphasis is placed on measurements of the optical constants at temperatures above 77 K. CO₂-ice occurs naturally on the surface and in the atmosphere of Mars,¹ where its temperature is probably ~ 150 K. Some of the measurements reviewed here were motivated by attempts to explain satellite measurements of radiation emitted and reflected by Mars.

At pressures below the triple point (5.2 atm), carbon dioxide exists only as a gas or solid. The sublimation point at 1-atm pressure is 195 K. Only one form of

solid CO₂ is known to occur naturally. A second crystal form, dry ice II, has recently been discovered in the laboratory at pressures above 5000 atm.² In this paper we are concerned only with the ordinary low-pressure form of CO₂ ice.

CO₂ crystallizes into a cubic space group,³ so it cannot exhibit birefringence. The optical constants are independent of the orientation of the crystal relative to the plane of polarization of the light.⁴ Measurements on polycrystalline samples, which was likely the case for all measurements reviewed here, are, therefore, adequate to describe the behavior of single crystals as well.

A. Features of the Spectrum

CO₂ ice exhibits a strong absorption continuum in the ultraviolet (50–130-nm wavelength) due to electronic transitions. It is relatively transparent in the visible region, but the absorption is not as weak in CO₂ ice as in H₂O ice, where k_{abs} is a factor of ~ 400 smaller. Absorption maxima in the IR occur in the solid at approximately the same wavelengths as in CO₂ gas, near 1.4-, 2-, 2.7-, 4.3-, and 15- μm wavelength, corresponding to vibrational transitions of the CO₂ molecule. The strongest peaks are those at 4.3 μm (asymmetric stretching ν_3) and 15 μm (bending ν_2), as in the gas. A weaker absorption feature occurs in the solid at the frequency of the ν_1 fundamental near 7- μm wavelength, but this is absent by reason of symmetry from the absorption spectrum of the gas except at very high pressure. There are two intense lines in the far-IR due to lattice vibrations near 90 and 150 μm .

The spectrum is characterized by very intense, very narrow absorption lines whose strength, location, and

The author is with University of Washington, Department of Atmospheric Sciences, Seattle, Washington 98195.

Received 21 November 1985.

0003-6935/86/162650-25\$02.00/0.

© 1986 Optical Society of America.

width are temperature-dependent, making both the measurements and compilation difficult. The absorption is very weak in the regions between the lines. Figure 4 of Fink and Sill⁵ compares the CO₂ spectrum with those of other ices (CH₄, H₂O, NH₃, NH₄SH, and H₂S), commenting that "the spectrum of CO₂ has the sharpest features of any solid we have observed." They attribute the contrast between the water-ice spectrum and the CO₂-ice spectrum to the lack of hydrogen bonding in CO₂ ice. Weaker interactions between molecules allow longer lifetimes for excited states and thus narrower absorption lines.

Although k_{abs} is very small between the absorption lines, it is not negligible. Accurate quantitative values of k_{abs} are needed even where it is small, because it affects the reflectance and emittance of planetary surfaces. Absorption of solar radiation by CO₂ snow can be quite significant (~30%) even in spectral regions where k_{abs} is 5–6 orders of magnitude smaller than in the strong bands.⁶ Some of the spectral channels used for remote sensing of the Martian surface by satellite also are located in the weakly absorbing regions between the lines.

Subsidiary peaks appear in the spectrum near the strong absorption lines due to the less common isotope ¹³C¹⁶O₂. If the measurements reviewed here are to be used for inferences about other planets, the assumption is implicit that the ¹³C/¹²C ratio is the same as on earth.

B. Difficulties of Measurement

The absorption coefficient k_{abs} (or the imaginary index m_{im}) is obtained by measurements of light transmission through clear crystals of CO₂. In spectral regions where m_{im} is large (≥ 0.01) it can also be obtained by reflectance measurements. The latter procedure has not been tried for CO₂ ice, except in the UV, perhaps because it is difficult to obtain a smooth surface on samples formed by condensation of gas onto a cold window. To obtain measurable transmission in the strong IR band at 4.3 μm , samples of 40–420-nm thickness were used,^{5,7} and in the UV some films only 20 nm thick were used.⁸

In the spectral regions of weak absorption, thicker crystals (several millimeters) are needed to obtain significant attenuation. As the crystals grow thicker by deposition, it becomes more difficult to keep them free from cracks. This is one reason for the paucity of measurements of k_{abs} between the strong lines. Egan and Spagnolo⁹ were able to prepare clear samples only by adding small amounts of water and mineral oil. They also found it important to polish the samples to avoid light scattering from a rough surface. According to them, "If optically clear dry ice was not selected, the imaginary portion of the complex index could be [erroneously computed to be] higher by a factor of ten because of the greater amount of light scatter."

A method for growing clear thick samples of pure CO₂ without additives was mentioned by Behn.¹⁰ This method was modified and described in detail by Gaizauskas,¹¹ who used it to grow CO₂ ice for measure-

ments of the weak ν_1 band. It was used by subsequent workers in the same laboratory,^{12,13} but it appears not to have been tried by workers elsewhere. For example, Ditteon and Kieffer¹⁴ were unable to report accurate values of m_{im} in the weakly absorbing regions of the IR because their samples were cracked and also had a rough surface, so that the attenuation of light due to scattering was very likely greater than that due to absorption in many parts of the spectrum they measured.

Another experimental difficulty is the need for very high spectral resolution in the vicinity of the strong lines. The data of Fink and Sill⁵ show that some of the absorption lines have halfwidths $< 1 \text{ cm}^{-1}$ in wave number. The measurements by most other authors were made with spectral resolution coarser than 1 cm^{-1} , so they did not resolve the peaks adequately.

A final difficulty in describing the absorption spectrum is the fact that the positions, strengths, and widths of the lines are temperature-dependent, generally broadening as the temperature T is increased. This means that an adequate description of $m(\lambda, T)$ will require measurements of k_{abs} at several temperatures for each wavelength. Such a complete description is not now available. Most parts of the spectrum have been measured only at one temperature. Here we accept data from measurements at any temperature $T > 77 \text{ K}$ (in the UV we accept measurements also at lower temperatures) and do not attempt to describe the temperature dependence because of lack of information.

The real index m_{re} can be obtained by measurements of reflection or refraction (or by counting interference fringes in thin films) in spectral regions where m_{im} is small enough that it does not affect the reflectance. This has been done in the visible region by several authors. At other wavelengths, m_{re} can be obtained by Kramers-Kronig analysis if $m_{\text{im}}(\lambda)$ is known for the entire spectrum:

$$m_{\text{re}}(\lambda_0) = 1 + \frac{2\lambda_0^2}{\pi} P \int_0^\infty \frac{m_{\text{im}}(\lambda) d\lambda}{\lambda(\lambda_0^2 - \lambda^2)}, \quad (1)$$

where P indicates the Cauchy principal value of the integral.

C. Compilation Procedure

The approach used in my recent review of optical constants of water ice¹⁵ is also used here. Measurements of m_{im} are reviewed and displayed in figures to illustrate the differences that exist between experiments in different laboratories. Transmission data from the cloudy sample of Ditteon and Kieffer¹⁴ in the IR are reanalyzed by means of subsequently available constraints on the real index and by forcing their m_{im} to agree as closely as possible with that measured on a clear sample by Gaizauskas¹¹ in the 6–9- μm spectral region, where the two sets of measurements overlap. The reanalysis involves estimation of a wavelength-dependent scattering coefficient $k_{\text{scat}}(\lambda)$ for the cloudy sample.

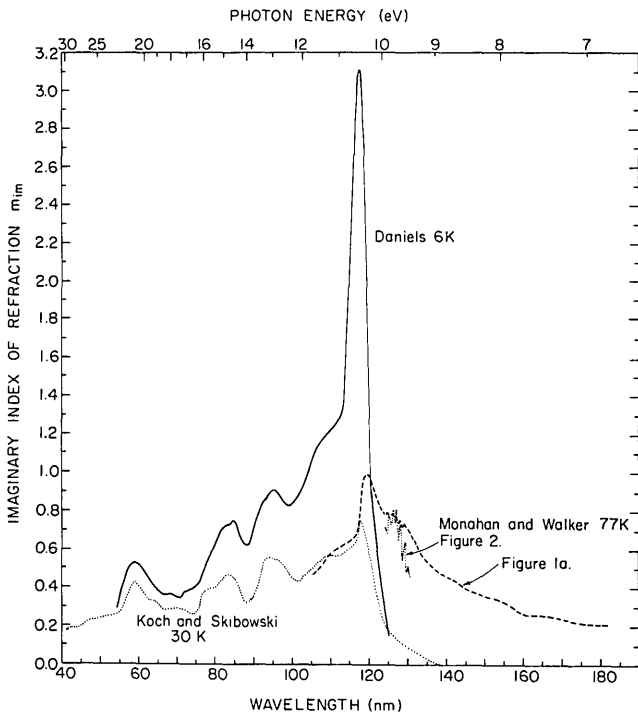


Fig. 1. Imaginary refractive index of CO₂ ice in the UV. Our compilation uses the values of Daniels, scaled down by 4% to obtain the observed m_{Re} in the visible, as explained in Sec. VII.A.

A trial function $m_{Im}(\lambda)$ is then constructed to be used in Eq. (1). In this trial function, however, $m_{Im}(\lambda)$ in the 4.3- and 15- μm bands was obtained from transmission data of Yamada and Person⁷ by assuming that (after subtracting a background spectrum) the attenuation was due entirely to absorption, not to reflection. This assumption by Yamada and Person is incorrect; m_{Im} is so large here that it causes m_{Re} to vary greatly across the band according to Eq. (1), causing the reflectivity of the air-CO₂ and window-CO₂ interfaces to vary with wavelength. Our procedure, therefore, involves (1) scaling of the x ray or ultraviolet m_{Im} to obtain the correct m_{Re} for visible wavelengths (because m_{Re} in the visible is better known than m_{Im} in the x ray and UV); (2) a computation of reflectivity of Yamada and Person's sample using a trial real index function $m_{Re}(\lambda)$ and redetermination of $m_{Im}(\lambda)$ from the transmission data at 4.3 and 15 μm ; and (3) a computation of real index over the entire spectrum by Eq. (1). Steps (1), (2), and (3) are iterated to convergence.

More discussion of the Kramers-Kronig analysis methods, as well as the numerical procedures, are given in the parallel article on H₂O ice.¹⁵

The self-consistent set of $m_{Im}(\lambda)$ and $m_{Re}(\lambda)$ are then tabulated for much of the spectrum. There are gaps in the table of m_{Im} in some spectral regions of weak absorption where no measurements have been made. However, m_{Re} is tabulated even in those regions because it can be obtained reliably from Eq. (1), since data on m_{Im} are lacking only in regions where m_{Im} is so small that it does not affect m_{Re} . It turns out that m_{Re} is close to 1.4 for all parts of the spectrum except near strong absorption bands.

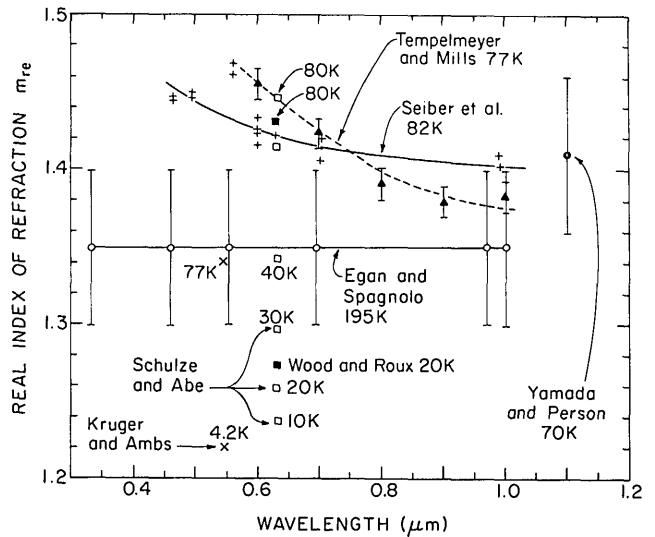


Fig. 2. Real refractive index of CO₂ ice in the visible and near visible. Open circles with error bars, Egan and Spagnolo⁹; solid circle with error bar, Yamada and Person⁷; triangles with error bars, Tempelmeier and Mills,²⁸ with the dashed line showing their fit to the data; +, Seiber *et al.*²⁵ with solid line showing their fit to the data; ×, Kruger and Amb²⁹ measurements at two condensation temperatures; □, Schulze and Abe³⁰ condensed at the temperatures indicated. (Their measurements were made at many temperatures, but only six representative points are shown here.) ■, Wood and Roux,³¹ measurements at two condensation temperatures. Our compilation uses the upper solid line, fitting the measurements of Seiber *et al.*, to obtain a reference value of $m_{Re} = 1.404$ at $\lambda = 1.0 \mu\text{m}$ for use in the Kramers-Kronig analysis.

II. Ultraviolet and X Ray

A. Sources of Data

Koster¹⁶ (1971) measured the oxygen K -emission band of CO₂ ice, which is located in the soft x-ray region of 2.3–2.4-nm wavelength as it is in water ice.¹⁵ No absolute values of absorption coefficient were given. We use the spectral shape of k_{abs} obtained by Koster and scale the absolute values below to obtain the correct value of m_{Re} in the visible when the Kramers-Kronig (KK) analysis is done.

Daniels¹⁷ (1970) measured the energy loss of 60-keV electrons beamed onto a thin film of CO₂ (~200 nm thick) at 6 K. He obtained ϵ_{Re} and ϵ_{Im} by dispersion analysis¹⁸ over the 52–125-nm wavelength range. The corresponding $m_{Im}(\lambda)$ is plotted in Fig. 1. His spectral resolution was 0.1 eV, which corresponds to 0.2 nm in wavelength at $\lambda = 52$ and 1.3 nm at $\lambda = 125$ nm. [Daniels' plot of ϵ_{Re} in his Fig. 2(b) is broken at 11 eV. One section of the curve has the notation ×10. This does not mean that the values have been multiplied by 10 but instead is apparently an instruction to the reader that the plotted values need to be multiplied by 10. This ambiguity was resolved during the KK analysis described below; the alternative interpretation caused gross disagreement with our derived m_{Re} .]

Koch and Skibowski¹⁹ (1972) (KS) measured the reflection spectrum of CO₂ at 30 K, from 40 to 140 nm, using polarized synchrotron radiation as the UV light source. KS applied KK analysis to the reflection spec-

trum to obtain ϵ . To do this they assumed that m_{Re} (visible) = 1.22, somewhat lower than the value of 1.4 we find below. Unfortunately, KS plotted only ϵ_{Im} , not ϵ_{Re} , but we need both to obtain m_{Im} .

Three attempts are made to infer m_{Im} from the published data: (1) KS plots of $\epsilon_{Im}(\lambda)$ and reflectivity $r(\lambda)$ are used to find an $\epsilon_{Re}(\lambda)$ consistent with them via the Fresnel equations.²⁰ However, when the resulting $m_{Im}(\lambda)$ is used in a KK analysis of the entire spectrum, the ϵ_{Re} which is computed is different than that used in deriving m_{Im} . This inconsistency is probably due mainly to the difficulty of reading values accurately off the small graph in the KS published paper. (2) The published reflectance is analyzed²¹ to infer ϵ . This procedure (also used by KS) is not definitive because it is very sensitive to the assumption made about the low-frequency wing of $r(\lambda)$. (3) The KS reported values of $\epsilon_{Im}(\lambda)$ are used in a KK analysis of the entire spectrum (after the remainder of the spectrum has been constructed), using Eq. (17.10b) of Stern,²² modified in analogy to Eq. (3) of Warren.¹⁵

Subsequent to these attempts to infer m_{Im} , the values of $\epsilon_{Re}(\lambda)$ which had been obtained by KS but not published in their paper were kindly supplied by Koch. The $m_{Im}(\lambda)$ corresponding to KS values of ($\epsilon_{Re}, \epsilon_{Im}$) is plotted in Fig. 1 and is used below in the KK analysis of the entire spectrum. It agrees with the values obtained in procedure (3) of the previous paragraph.

The explanation of the spectrum measured by KS, in terms of electronic structure, was recently reviewed by Fock *et al.*²³

Monahan and Walker⁸ (1974) (MW) measured transmission through films of CO₂ 20–40 nm thick at 77 K from 106- to 182-nm wavelength. Surface reflectance varies with wavelength in this region, and MW corrected for it “by comparing the transmitted intensities for two films of different thickness.” The formula they gave for doing this [their Eq. (1)] is incorrect; probably it is a misprint. (The equation was given correctly in a subsequent paper.²⁴) MW obtained this difference in thickness not by direct measurement but rather by calibration against the optical constants of KS in the region where they overlapped. Details of the band structure at 125–130 nm shown in their Fig. 2 do not agree with $k_{abs}(\lambda)$ plotted in their Fig. 1(a). In Fig. 1 here we plot the corresponding m_{Im} from both of their figures. Even though MW stated that they scaled their k_{abs} to match that of KS, the two disagree considerably from 118 to 140 nm. The subsequent measurements²⁴ by MW are useless to us because the difference in thickness between the two samples was not given.

B. Compilation of Imaginary Index

We choose to ignore the data of MW because of (a) lack of agreement between MW Fig. 1(a) and MW Fig. 2, (b) the fact that the MW peak in m_{Im} does not occur at the 118-nm wavelength found by both Daniels and KS, and (c) the fact that MW showed continued large absorption ($m_{Im} > 0.2$) out to 180 nm, in disagreement with the rapid drop in absorption to near zero found by

both Daniels and KS at ~ 125 nm.

It is difficult to choose between the values of Daniels and those of KS. Daniels m_{Im} is larger everywhere but especially in the peak at 118 nm. Since this is an electronic transition, it seems unlikely that this huge difference could be due to the change of temperature from 6 to 30 K. A possible experimental error which could cause KS values to be too low is a rough surface on their sample, which might scatter light in other directions than toward the detector so that the measured reflectance would be too low. If the Daniels values are correct, the KS reflectivity is a factor of 1.6 too low at 20 eV and a factor of 3 too low at 10 eV.

However, there is evidence that this peak at 118 nm is quite large at higher temperature. The favored measurements of $m_{Re}(\lambda)$ is the visible described in Sec. IIIA show m_{Re} (at $T = 80$ K) increasing as wavelength decreases (the values of Seiber *et al.*²⁵ shown in Fig. 2). The magnitude of this increase implies a peak even larger than Daniels reported. An alternative explanation of the wavelength-dependence of visible m_{Re} would be a strong absorption band in the 180–330-nm spectral region, a region which has never been investigated. However, that seems unlikely because the spectrum of CO₂ gas²⁶ shows only weak absorption throughout this region, with average absorption coefficients a factor of 100 smaller than those in the 50–130-nm region.

On the other hand, evidence in favor of a small peak at 118 nm at higher temperatures can be found in the transmission measurements of Abe and Onaka²⁷ at $T = 77$ K. They did not measure their sample thickness, so it is unknown how much of their optical density is due to reflection as m_{Re} varies through the spectrum. However, their spectrum shows the peak at 118 nm rising above its background to about the same extent as found by KS (Fig. 1). (The measurements of MW plotted in Fig. 1 are not evidence in favor of KS; they were intentionally scaled by MW to agree with KS as mentioned above.)

For the compilation we use Daniels $m_{Im}(\lambda)$ because of the evidence from $m_{Re}(\lambda)$ in the visible. However, because of the difficulty of choosing between the m_{Im} of Daniels and that of KS, separate KK analyses are performed below using each of them to compute two sets of $m_{Re}(\lambda)$. These $m_{Re}(\lambda)$ differ only for $\lambda \lesssim 0.6$ μm . They are both plotted below for the UV region so that the reader can choose either.

III. Visible and Near-Visible, 0.3–1.1 μm

A. Real Index

Although we will compute $m_{Re}(\lambda)$ using Eq. (1), we need at least one experimentally measured value as a reference value at a wavelength where $m_{Im} \ll 1$, because the absolute intensity of the x-ray band is unknown. The real index has been measured in the visible region by several authors, whose results are shown together in Fig. 2. Egan and Spagnolo⁹ measured the Brewster angle and found m_{Re} constant at 1.35 ± 0.05 across the visible. Yamada and Person⁷

measured the intensity of interference fringes and found $m_{Re} = 1.41 \pm 0.05$ at $\lambda = 1.1 \mu\text{m}$ and $T \approx 70 \text{ K}$. Tempelmeyer and Mills²⁸ located interference fringe maxima as a function of sample thickness at $T = 77 \text{ K}$ finding m_{Re} to decrease as wavelength increases. Seiber *et al.*²⁵ (in the same laboratory) later used the same method at 82 K obtaining somewhat weaker dependence of m_{Re} on λ and explained why their measurements were likely to be more accurate than those of Tempelmeyer and Mills.

The dependence of m_{Re} on condensation temperature was investigated first by Kruger and Ambs²⁹ for only two temperatures and more thoroughly by Schulze and Abe³⁰ for temperatures of 4–86 K (at the single wavelength $\lambda = 0.633 \mu\text{m}$). The refractive index increases with deposition temperature because the crystal structure is porous and the CO_2 ice is less dense when the gas is condensed at lower temperature. Schulze and Abe showed that m_{Re} (at $\lambda = 0.633 \mu\text{m}$) became relatively independent of temperature above 78 K, stabilizing at $m_{Re} = 1.45$. Their results are undoubtedly dependent on the mode of formation of the crystal (by condensation of gas). It seems unlikely that such a large variation of m_{Re} with temperature would be seen for a CO_2 -ice block which was formed at high temperature and subsequently cooled, but such measurements have not been reported. Wood and Roux³¹ measured m_{Re} for CO_2 condensed at 20 and 80 K at $\lambda = 0.633 \mu\text{m}$, in qualitative agreement with the temperature dependence found by Schulze and Abe.

All the authors who made measurements at temperatures near 80 K agree to ± 0.05 . Seiber *et al.*'s measurement of the wavelength dependence is supported by results of Yamada and Person as well as Wood and Roux. We select the results of Seiber *et al.* as the reference value of m_{Re} for use in the KK analysis. We ignore the data of Egan and Spagnolo⁹ at 195 K because of their large uncertainty, but they raise the possibility that m_{Re} may be somewhat lower at high temperatures.

The observed increase of m_{Re} with decreasing wavelength is caused by the strong UV absorption band. If we use the m_{Im} of KS in the UV, we obtain $m_{Re} = 1.427$ at $\lambda = 0.3 \mu\text{m}$ and $m_{Re} = 1.408$ at $\lambda = 0.6 \mu\text{m}$, whereas Daniels m_{Im} causes $m_{Re} = 1.448$ and 1.411, respectively. Our choice of Daniels data for the UV thus causes a steeper dependence of m_{Re} on λ in the visible but still not as steep as the dependence observed by Seiber *et al.*

B. Imaginary Index

The only measurements of absorption by CO_2 ice in the visible were made by Egan and Spagnolo⁹ (ES). They used commercial dry ice which contained 50 ppm of water and 50 ppm of mineral oil to reduce cracking and light scattering. These impurities were thought to cause negligible absorption in the wavelengths studied. Clear blocks $\sim 10 \text{ mm}$ thick were selected and polished. Transmission at each wavelength was measured for many different thicknesses at $T = 195 \text{ K}$ as the CO_2 sublimed away. The effects of reflection

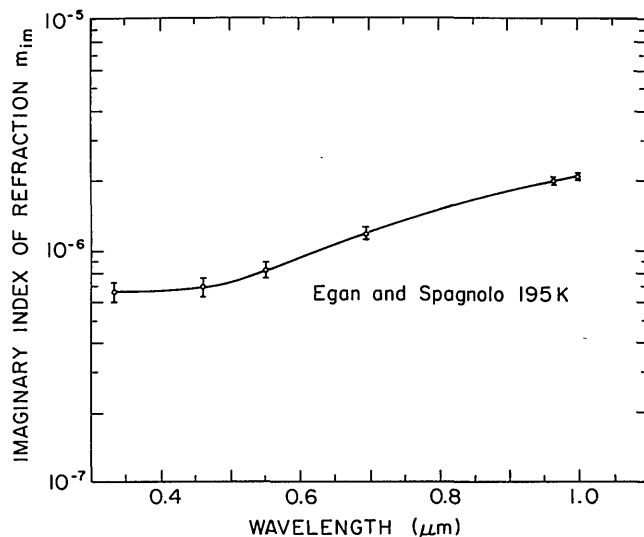


Fig. 3. Imaginary refractive index of CO_2 ice in the visible and near visible. Measurements were made by Egan and Spagnolo⁹ at the six wavelengths indicated; the solid line is their interpolation.

could thus be eliminated in the analysis, and k_{abs} could be obtained from the slope of $\log(\text{transmission})$ vs sample thickness at each wavelength; two examples were given in ES's Fig. 1. The complete plot of κ vs λ was given in their Fig. 2, where $\kappa \equiv m_{Im}/m_{Re}$. The slopes in ES's Fig. 1 imply values of κ a factor of 20 larger than those in their Fig. 2, suggesting a mislabeled scale. According to Egan (personal communication), Fig. 2 is correct, whereas Fig. 1 "was arbitrarily normalized to show the points of two curves separated yet not having the curves intersecting." Further evidence favoring Fig. 2 of ES over their Fig. 1 comes from the visual transparency of CO_2 ice seen by Behn¹⁰ and by Egan (personal communication). The m_{Im} corresponding to ES's Fig. 2 is plotted here in Fig. 3 and used in the compilation.

The fact that commercial dry ice was used without purification is a cause for concern. Trace amounts of absorptive impurities introduced during the manufacturing process could cause large errors in the measured absorption because CO_2 is relatively transparent in this spectral region. For example, if ES's sample contained more than 0.5 ppm of carbon, the absorption due to the carbon would be greater than that due to the CO_2 in the sample. The factory which manufactured the dry ice used by ES is no longer in operation, so we are unable to inquire about this possibility. Such impurities would have been left behind as a deposit on the surface of the remaining sample as the CO_2 sublimed away during the experiment, and the plots of $\log(\text{transmission})$ vs sample thickness (ES Fig. 1) would be concave downward (rather than straight lines) if the impurities had absorbed light significantly. The curvature would be greater at wavelengths where CO_2 is less absorptive. There is just a suggestion of such behavior in Fig. 1 of ES: the plot for $0.46 \mu\text{m}$ is indeed concave downward, whereas that for the more absorptive wavelength $1.0 \mu\text{m}$ is not; but there really is too much scatter in the data to rule out a

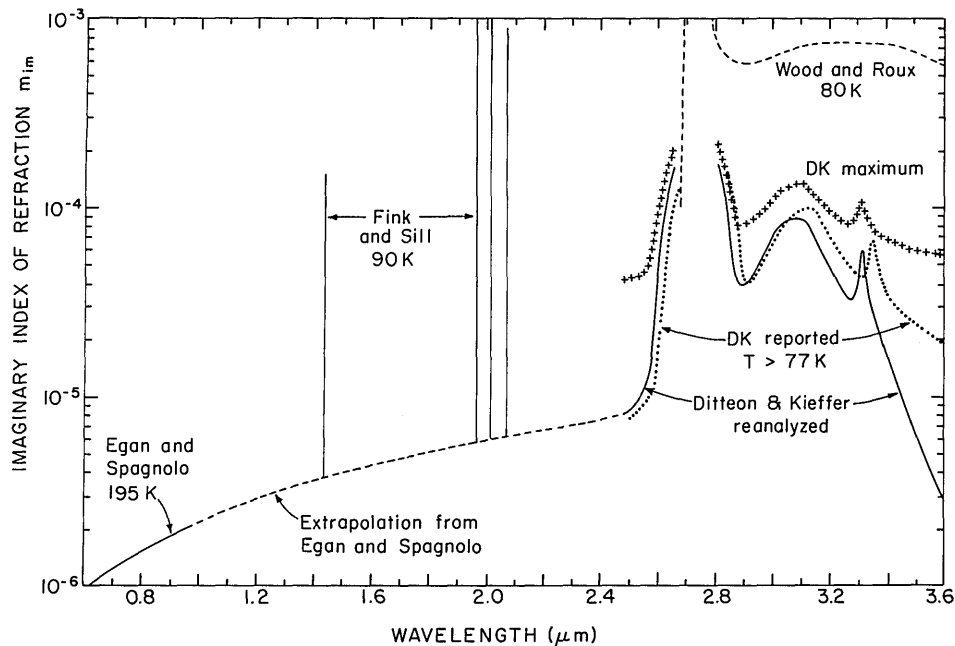


Fig. 4. Imaginary index of refraction of CO_2 ice in the near infrared. The four narrow lines measured by Fink and Sill⁵ near 1.4 and 2.0 μm are resolved with an expanded scale in Fig. 5. The individual data points of Wood and Roux³¹ are not shown; our smoothed fit to them (dashed line) was not drawn to match them in detail because Wood and Roux's measured values of m_{im} are very uncertain when they are below 10^{-3} . Ditteon and Kieffer's¹⁴ (DK's) published m_{im} is shown as the dotted line; our reanalysis of DK's transmission data as a solid line; and the maximum possible m_{im} from DK's data (i.e., assuming no scattering by their sample) as the line of plus signs. The reanalysis used the scattering coefficients plotted in Fig. 11. Our compilation uses the extrapolation from Egan and Spagnolo⁹ (dashed line), the four narrow lines of Fink and Sill,⁵ and the reanalysis of Ditteon and Kieffer (solid lines at the right). Data of Wood and Roux³¹ are used between 2.68 and 2.782 μm ; interpolation is described in the text.

straight-line fit to each. Egan (personal communication) did not see any deposits of dust when visually examining the samples.

IV. Near- and Middle-Infrared, 1.4–25 μm

The IR spectrum is characterized by very intense narrow absorption features separated by regions of very weak absorption. The laboratory experiments are readily separated into those which measured only the strong absorption bands and those which measured only the weakly absorbing regions. The same bands which are strongly absorbing in CO_2 gas are also strong in the solid. These are the fundamental vibrational modes ν_2 at 15 μm and ν_3 at 4.3- μm wavelength as well as weaker bands at 1.4, 1.9, 2.0, 2.1, and 2.7 μm . The fundamental symmetric-stretching mode ν_1 at 6–9 μm is inactive in the gas but appears as a weak absorption band in the solid due to interaction with lattice vibrations.^{11–13}

A. Strong Absorption Bands

1. Sources of Data

Fink and Sill⁵ (1982) (FS) measured transmission spectra for several low-molecular-weight ices thought to be possible constituents of comets. Eight films of CO_2 ice were used with thicknesses from 0.04 to 69 μm at temperatures ~ 90 K (Fink, personal communication). Preliminary values of the Lambert absorption

coefficient k_{abs} were plotted in their Fig. 4 for 2.6–100 μm ; the numerical values were kindly supplied by Fink (personal communication) for the published figure as well as for shorter wavelengths down to 1.4 μm . The uncertainty in k_{abs} was generally $\sim 20\%$, the wavelength resolution < 1 cm^{-1} . The samples were so thin that values of k_{abs} could only be obtained in the strong absorption bands. The description of the experimental method (Appendix of Ref. 32) made no mention of the fact that m_{Re} can vary dramatically across an absorption band, so we assume that these values of k_{abs} were obtained simply as

$$k_{\text{abs}} = (1/d) \ln(I_B/I_S), \quad (2)$$

where d is sample thickness and I_B and I_S are the transmitted intensities of the blank cell and with the sample in place, respectively. Since reflectance varies with wavelength in the 4.3- and 15- μm bands, this procedure leads to erroneous results in those bands, as shown below.

Figure 4 shows the absorption features measured by FS in the 1.4–2.1- μm region. They are too narrow to be resolved in Fig. 4 so they are displayed in Fig. 5 on expanded wavelength scales. Data from FS are also plotted in Figs. 6, 7, and 8 for the bands at 2.7, 4.3, and 15 μm , respectively.

Since FS did not plot their raw transmittance data and since their reported k_{abs} is a composite result of measurements on samples of different thickness, it is

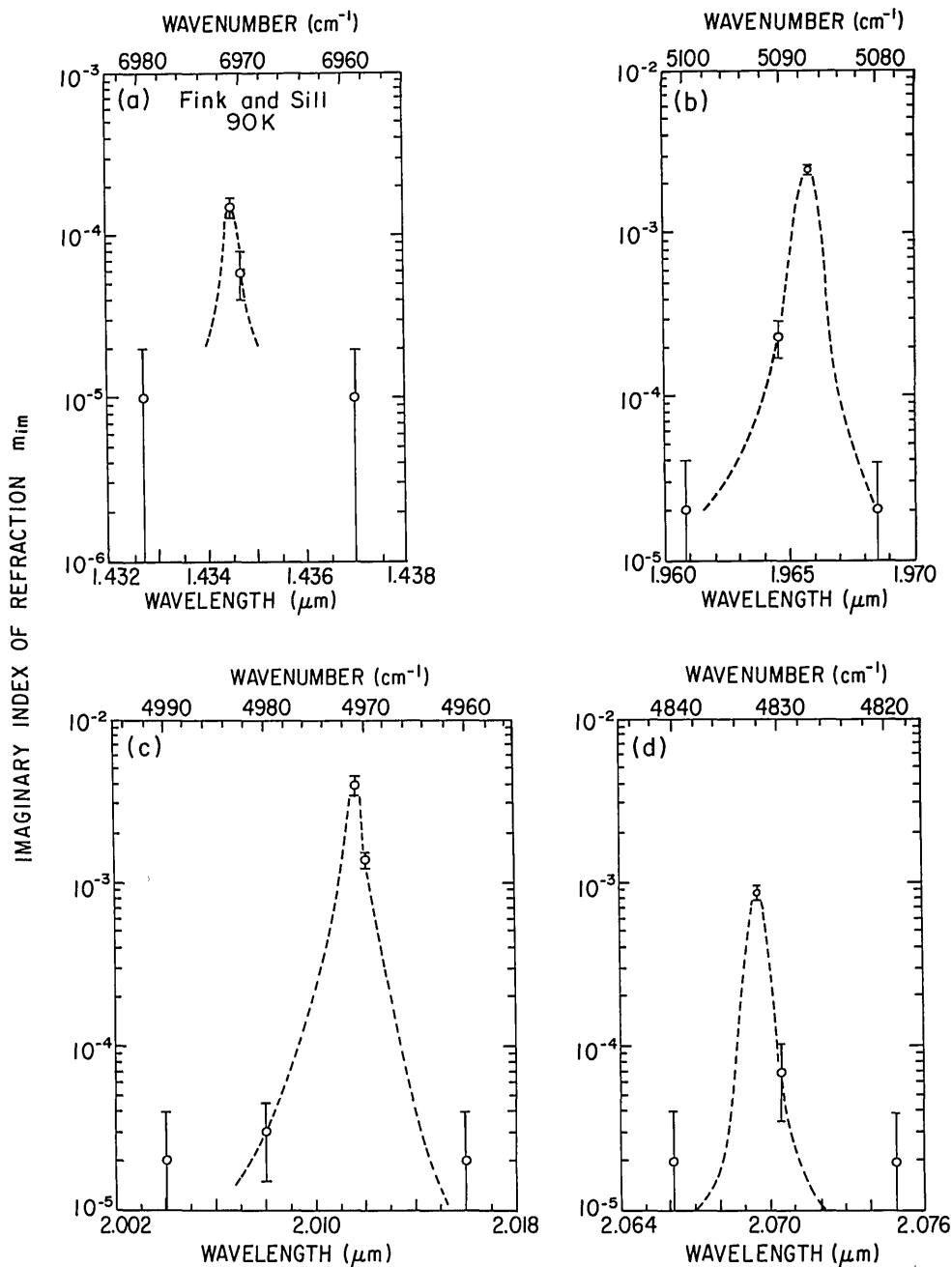


Fig. 5. Details of the four narrow near-IR absorption lines near 1.4 and 2.0 μm . Our compilation uses the dashed lines which we fit to the data points of Fink and Sill.⁵ In drawing the lines we ignore the low-valued data points in the wings because of their large uncertainty. Numerical values were kindly supplied by U. Fink (personal communication) with the caution that they are preliminary.

not possible to reinterpret the published data (taking into account variation of m_{Re} across the peaks) in the manner we do for Yamada and Person's data below. For this reason the FS measurements are used in the compilation only in spectral regions where there are no measurements available from other sources. If the original measurements of FS are properly reinterpreted in the future, they will probably supersede the measurements of other authors because of the finer spectral resolution of FS.

Yamada and Person⁷ (1964) (YP) studied the strong bands at 4.3 and 15 μm . They measured transmission through samples $<1 \mu\text{m}$ thick at temperatures of 65–80 K formed by deposition of CO_2 gas onto cold

windows. The sample thicknesses were obtained by measuring interference fringes outside the strongly absorbing regions (at $\lambda = 1.1 \mu\text{m}$). The wavelength resolution was 1 cm^{-1} at 15 μm and $\sim 2 \text{ cm}^{-1}$ at 4.3 μm ; the frequency calibration used the known line spectra of several gases. The experimental method was given in more detail in an earlier paper.³³ YP claimed that Eq. (2) could be used to obtain k_{abs} , which would be true if the real refractive index of CO_2 did not change across the absorption band. However, both ν_2 and ν_3 are intense enough to cause m_{Re} to vary substantially (from 0.3 to 3.2, as shown below) across the absorption peaks causing substantial reflection at the CO_2 -air and CO_2 -window interfaces at some wavelengths in the

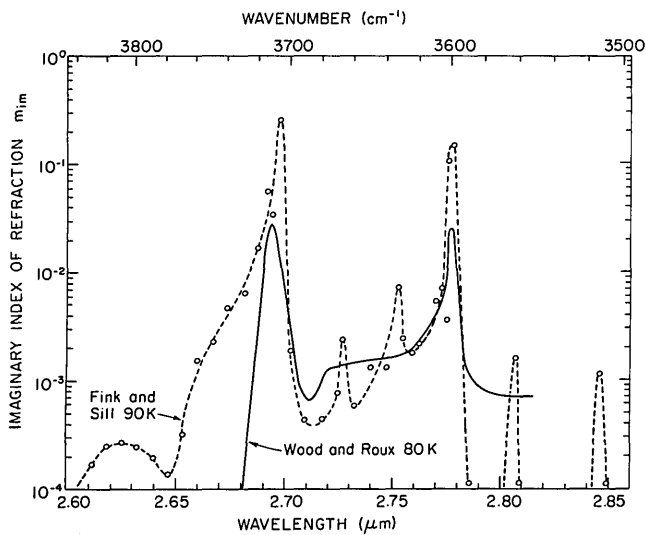


Fig. 6. Imaginary refractive index of CO_2 ice in the 2.7- μm absorption band. Fink and Sill's⁵ measurements are the open circles; the dashed line is our fit to those points. The compilation uses the data of Wood and Roux.³¹

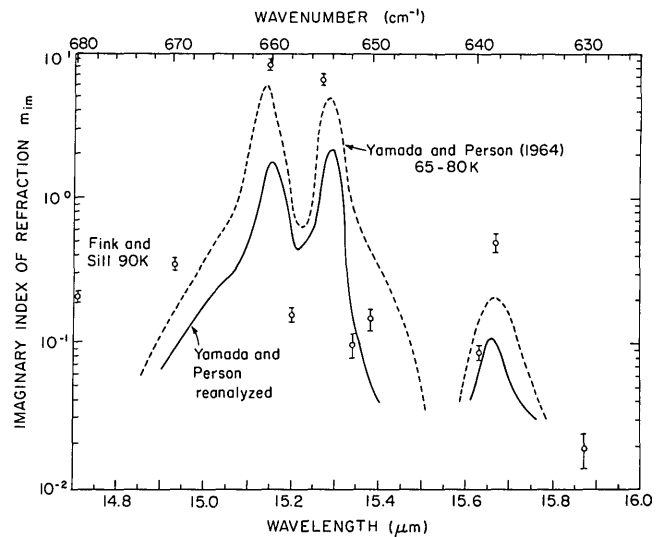


Fig. 8. Imaginary refractive index of CO_2 ice in the 15- μm absorption band. Neither Fink and Sill⁵ nor Yamada and Person⁷ subjected their transmission data to Kramers-Kronig analysis. Reanalysis of Yamada and Person's transmission data using Kramers-Kronig relations, described in Sec. VII.B, resulted in the solid line, which is used in the compilation.

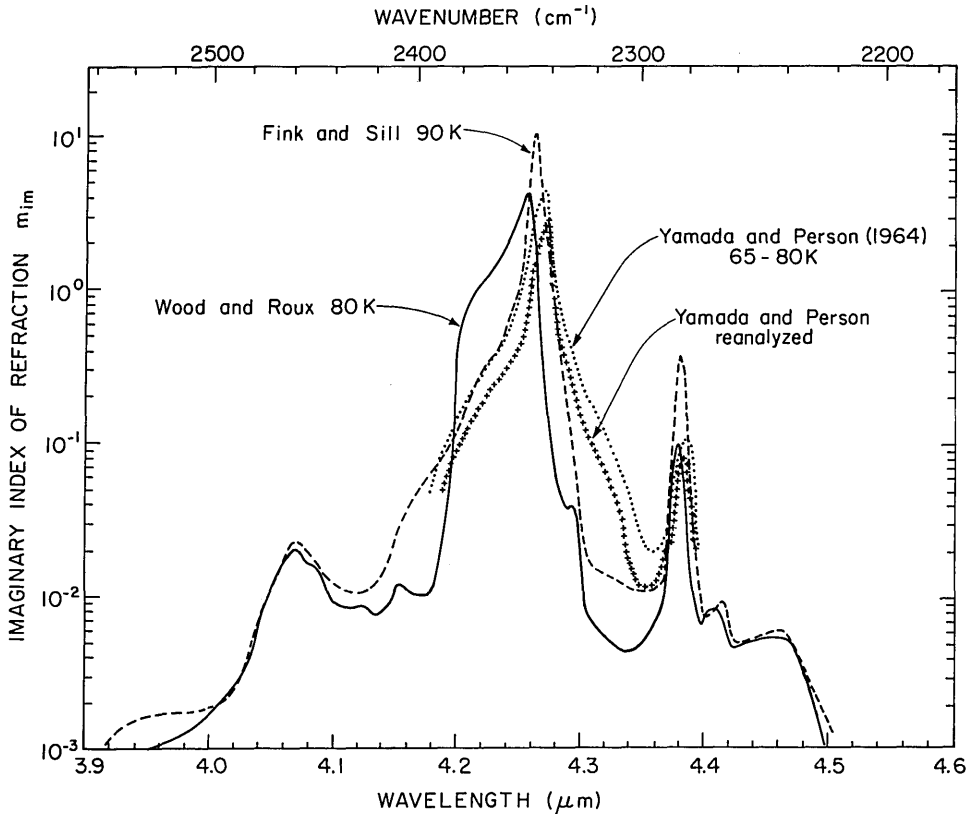


Fig. 7. Imaginary refractive index of CO_2 ice in the 4.3- μm absorption band. Wood and Roux³¹ took into account the variation of real index across the band when analyzing transmission data to obtain these results; the other authors did not. Our reanalysis of Yamada and Person's⁷ transmission data using Kramers-Kronig relations, described in the Appendix, resulted in the line of plus signs, which is used in the compilation.

absorption band, meaning that the reduced transmission with the sample in place should not be attributed entirely to absorption.

After subtracting the apparent background from Fig. 2 of YP, an uncorrected $k_{\text{abs}}(\lambda)$ is obtained using Eq. (2), and the corresponding $m_{\text{Im}}(\lambda)$ is plotted in Figs. 7 and 8. The transmission data are reinterpreted (after the remainder of the spectrum is constructed)

using Kramers-Kronig analysis of the entire spectrum to determine m_{Re} , and m_{Re} then to determine the reflectances of the interfaces, resulting (after several iterations) in the reanalyzed values of $m_{\text{Im}}(\lambda)$ also shown in Figs. 7 and 8. The detailed procedure is given in the Appendix. The minor peaks at 4.38 and 15.66 μm in these spectra are attributed⁷ to the isotope $^{13}\text{C}^{16}\text{O}_2$.

YP estimated an uncertainty of 10% for the integrated intensity of each band; specific values of $\ln(I_B/I_S)$ would have somewhat larger uncertainty. The tick marks on the YP wavelength axis are not uniformly spaced indicating a drafting error. This leads to a small uncertainty of up to $0.01 \mu\text{m}$ (0.4 cm^{-1}) in the positioning of the peaks in the $15\text{-}\mu\text{m}$ band and up to $0.002 \mu\text{m}$ (1 cm^{-1}) in the $4.3\text{-}\mu\text{m}$ band.

Wood and Roux³¹ (WR) condensed CO_2 gas to form thin films at both $T = 20$ and 80 K . We use the results at 80 K , for which 25 samples were measured, with thicknesses in the $0.23\text{--}13\text{-}\mu\text{m}$ range. Sample thickness was obtained by measuring interference fringes for visible light. Transmission measurements were made at wavelengths from 2.5 to $14.3 \mu\text{m}$, covering the strong bands at 2.7 and $4.3 \mu\text{m}$ but not at $15 \mu\text{m}$. The spectral resolution was 4 cm^{-1} , i.e., about twice as coarse as YP's. WR noted that the CO_2 spectrum changed more with temperature than did the spectra of H_2O and NH_3 .

Wood and Roux obtained m_{Re} and m_{Im} by a least-squares determination using several sample thicknesses. Then they applied KK analysis to this $m_{\text{Im}}(\lambda)$ to recompute $m_{\text{Re}}(\lambda)$. It is the latter $m_{\text{Re}}(\lambda)$ which is given in Table 6 of their report.³⁴ The KK-consistent $m_{\text{Im}}(\lambda)$ and $m_{\text{Re}}(\lambda)$ "yielded good agreement for all wavenumbers" when the transmittances implied by them were compared to the observed transmittance data. However, that statement seems incorrect for the center of the $4.3\text{-}\mu\text{m}$ band: WR's reported m implies 0.7% transmission for the thinnest sample, but their plot of transmission for this sample (Fig. 11 of Ref. 34) shows 6% transmission.

WR's $m_{\text{Im}}(\lambda)$ is plotted here (after some smoothing) in Fig. 6 for the $2.7\text{-}\mu\text{m}$ band and Fig. 7 for the $4.3\text{-}\mu\text{m}$ band. WR stated that their values of m_{Im} may be inaccurate wherever they are less than $\sim 10^{-3}$, because their samples were too thin to measure small absorption.

2. Choice of Data

In the rather weak narrow bands near 1.4 and $2.0 \mu\text{m}$ we use the values of FS; they are the only measurements available. In the $2.7\text{-}\mu\text{m}$ band (Fig. 6) the values of WR are favored over those of FS, because WR performed a KK analysis. However, the absorption peaks probably are actually narrower and higher, as found with FS's finer spectral resolution. FS's discovery of minor peaks at 2.73 , 2.75 , and $2.81 \mu\text{m}$ are also supported by the qualitative spectrum in Fig. 4 of Dows and Schettino.³⁵ However, these narrow peaks may broaden at higher temperature, so the coarse resolution data of WR may actually be more appropriate for planetary studies.

In the $4.3\text{-}\mu\text{m}$ band (Fig. 7) it is difficult to choose between the results of WR and the reanalysis of YP's transmission data. Although made at the same temperature, they disagree dramatically, with WR giving a larger total band strength and a prominent shoulder on the shortwave side of the peak. This shoulder does not appear in YP's measurements either before or after

reanalysis. The values of FS (also at about the same temperature) agree with those of YP both in the peak position and in the lack of a shoulder, but their peak value is considerably higher. Because the shape of YP's peak does not change much on reanalysis, we expect that Fink and Sill also would probably not obtain the shoulder if they were to reinterpret their transmission data. Such a shoulder is also absent in the absorption spectrum of CO_2 gas on the shortwave side of this band (Appendix 10 of Houghton³⁶).

The preliminary results of FS suggest that, on reanalysis, they would agree better with YP than with WR on the peak position and shape. However, they would agree better with WR for the integrated intensity. We use YP's data for the compilation. However, because of the difficulty of choosing between YP and WR, the complete KK analysis of the entire spectrum is performed in Sec. VII for each choice of data in the $4.3\text{-}\mu\text{m}$ band. The two sets of m_{Re} differ substantially only in the vicinity of the band; they are both plotted below so that the reader can choose either.

In fact, neither YP nor WR can have obtained values of m_{Im} to a high degree of certainty in the $4.3\text{-}\mu\text{m}$ band, because their thinnest samples ($\sim 0.23 \mu\text{m}$ in both cases) were still too thick to allow significant transmission at the band center, so that the observed transmission could contain a substantial contribution from leakage of light. YP obtained 4.5% transmission at the band center. As mentioned above, WR's reported m implies 0.7% transmission. Of the three experimental groups, only FS used a sample thin enough ($0.04 \mu\text{m}$) to obtain significant transmission here.

In the $15\text{-}\mu\text{m}$ band (Fig. 8) the measurements of YP are used. The values of FS are only for a few points, and (as explained above) it is not possible to reanalyze them properly using the available data. If YP and WR had agreed on the $4.3\text{-}\mu\text{m}$ band, that would give us confidence in the use of YP's data at $15 \mu\text{m}$. Since they did not agree, it would be desirable to obtain a second set of measurements for the $15\text{-}\mu\text{m}$ band. However, we can compare the locations of the peaks. YP and FS agree at $15 \mu\text{m}$ as they did at $4.3 \mu\text{m}$. WR made no quantitative measurements at $15 \mu\text{m}$ but did report the peak positions to be at 650 and 655 cm^{-1} , i.e., offset by $+5 \text{ cm}^{-1}$ from the positions found by YP and FS.

B. Regions of Weak Absorption

Gaizauskas¹¹ (1955) measured IR spectra of CO_2 gas, liquid, and solid. These include some of the most careful measurements ever made on CO_2 ice. The procedure for growing clear smooth thick crystals of purified CO_2 was discussed. Both Behn¹⁰ and Gaizauskas¹¹ were able to obtain them both from the liquid at high pressure and by deposition from the vapor at atmospheric pressure. Crystals grown from the liquid could not be used for the Gaizauskas IR measurements because the salt windows for IR absorption cells are too fragile to be used under pressure at low temperature. He, therefore, grew crystals from the gas following Behn's suggestion. The growth must be

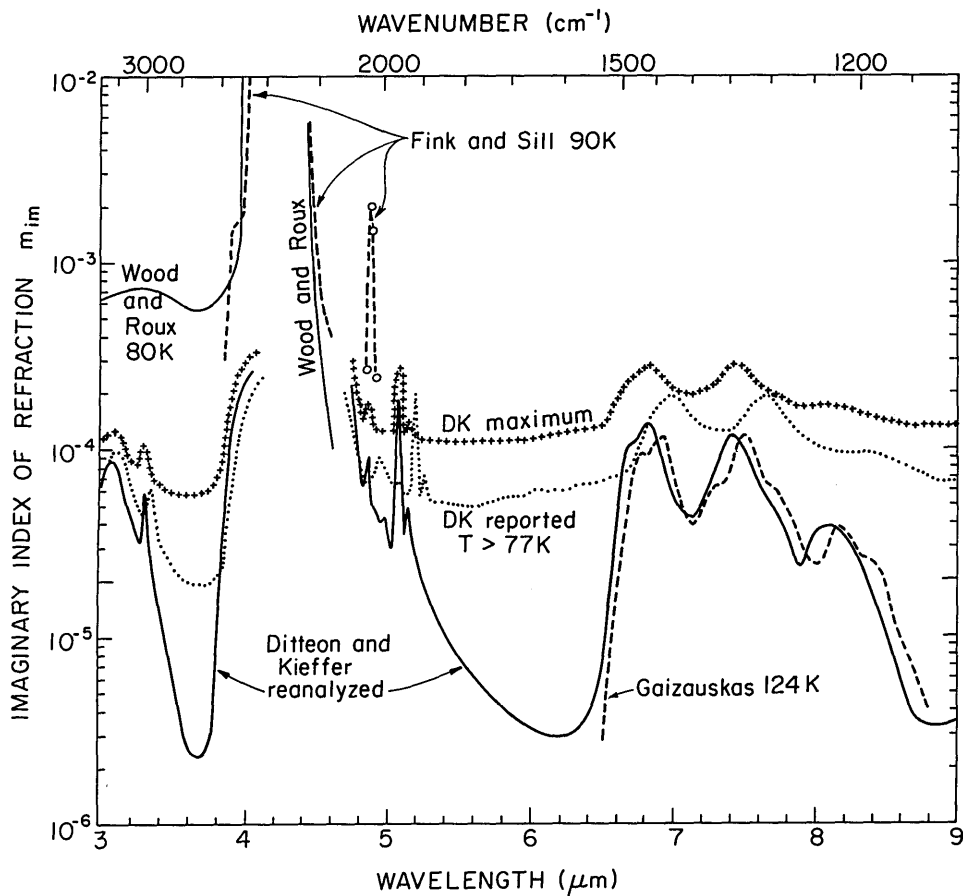


Fig. 9. Imaginary refractive index of CO₂ ice in the near and middle IR. The three plots of results from Ditteon and Kieffer¹⁴ are described in the legend to Fig. 4 and the text. The compilation uses DK-reanalyzed (solid curves) from 2.85 to 3.9 μm, Wood and Roux³¹ (upper solid curves) from 4.0 to 4.17 μm and from 4.4 to 4.5 μm, DK-reanalyzed from 4.8 to 6.54 μm, and Gaizauskas¹¹ from 6.64 to 8.76 μm.

done from CO₂ gas at nearly atmospheric pressure and the temperature systematically lowered as the crystal grows thicker.

Gaizauskas's main interest was to investigate to ν_1 band in all three phases of CO₂ (in the gas it is active only at high pressure), and he obtained quantitative absorption coefficients only for the 6–9-μm region (his Fig. IV-2) at $T = 124$ K. The spectral resolution was 3–5 cm⁻¹; the frequency calibration used the known line spectra of several gases. The corresponding m_{Im} is plotted here in Fig. 9. It is small enough that m_{Re} will not change significantly across this spectral region, so that we are able simply to use Eq. (2) to obtain k_{abs} and m_{Im} . The sample thickness, measured by microscope, was uncertain to ±10%, which causes the same fractional uncertainty in m_{Im} . The temperature dependence of this weak band was subsequently investigated by Blest-Castillo,¹² who, however, did not report absolute values of k_{abs} . The two highest peaks broadened somewhat as the temperature rose from 124 to 191 K. (A broadening of these peaks had also been shown earlier by Jacox and Milligan³⁷ as their sample warmed from 4 to 53 K.) Blest-Castillo also was successful at growing clear crystals by the same method used by Gaizauskas. Later work by Mannik and Allin¹³ at higher resolution ($\Delta\nu = 2$ cm⁻¹) obtained a more detailed structure in k_{abs} (their Fig. 3) with many minor peaks appearing that were not seen by Gaizauskas.

However, they reported no absolute values of k_{abs} , so their results are not plotted here.

Gaizauskas also recorded spectra of a CO₂-ice specimen "approximately 3 mm thick" for the 1900–2100-, 2650–3600-, and 4650–5400-cm⁻¹ regions (5.3–4.8-, 3.8–2.8-, and 2.2–1.9-μm wavelength, respectively) in his Figs. IV-4, 5, and 6. The ordinates of those figures are proportional to intensity but are uncalibrated. Since his thesis does not include spectra of the corresponding blanks, we cannot derive values of k_{abs} from those figures. [The blank spectra may have been recorded, but they no longer exist according to Gaizauskas (personal communication).] The absorption peaks in the 1.9–2.1-μm region in Gaizauskas' Fig. IV-6 are much broader than Fink and Sill⁵ reported; this is due to the coarse resolution (20 cm⁻¹) of Gaizauskas' instrument in this region compared with ~1 cm⁻¹ for Fink and Sill's instrument.

Ditteon and Kieffer¹⁴ (1979) (DK) used 4.2- and 1.7-mm thick deposits of CO₂ to measure transmission spectra in the weakly absorbing regions from 2.5- to 28-μm wavelength. Their principal difficulty was that the samples scattered light. Some crystals were initially clear, but they developed cracks and surface roughness during the course of the experiment due to lack of temperature control. The light scattering thus increased during the course of the spectral scan, and the samples also thinned by a few percent due to sublimation (Ditteon; personal communication).

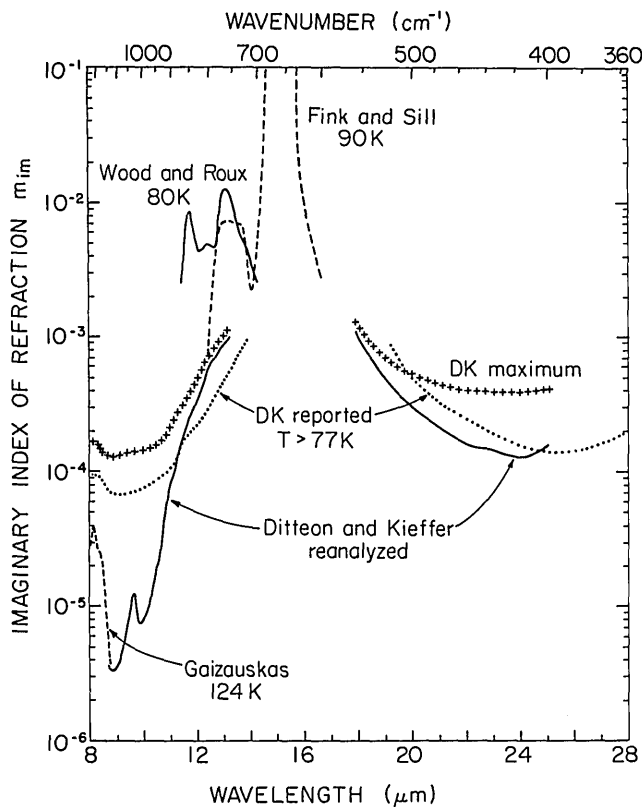


Fig. 10. Imaginary refractive index of CO₂ ice in the middle infrared. The three plots of results from Ditteon and Kieffer¹⁴ are described in the legend to Fig. 4 and the text. The compilation uses Gaizauskas¹¹ from 6.64 to 8.76 μm, DK-reanalyzed from 9.0 to 11.0 μm, Wood and Roux³¹ from 11.5 to 13.9 μm, Fink and Sill⁵ from 13.9 to 14.5 μm and 15.9 to 16.2 μm, and DK-reanalyzed from 17.9 to 25 μm.

DK took account of the scattering when they analyzed the data to obtain the optical constants. They found evidence that the scattering was inversely proportional to wavelength. They then used the two samples with two different scattering functions to obtain m_{Re} and m_{Im} at each wavelength.

The values of m_{Im} obtained by DK are plotted here in Figs. 4, 9, and 10. However, there are constraints available which allow more accurate interpretation of the data than they presented. DK's Fig. 4(a) shows m_{Re} to wiggle substantially in the 5–10-μm region, where there are no strong absorption bands that could cause such behavior, according to eq. (1). Both m_{Re} and m_{Im} were obtained by DK in a concerted analysis (a separate analysis at each wavelength), so the fact that their m_{Re} is wrong means that their m_{Im} is also wrong. Now that Wood and Roux³¹ have obtained $m_{Re}(\lambda)$, DK's measurements can be reanalyzed. Wood and Roux's m_{Re} is close to 1.4 except near the absorption bands, whereas DK obtained values of m_{Re} as high as 2.0 in the 6–9-μm region.

A further difficulty is that DK's measurement of wavelength appears to be in error. In regions where DK's measurements overlap those of other investigators, the locations of DK's absorption peaks appear at longer wavelengths, as shown here in Figs. 4, 9, and 10.

The difference averages 40 cm⁻¹. Since all the other sources agree with each other as to the locations of the absorption peaks, we conclude that DK's entire spectrum should be shifted 40 cm⁻¹ to higher frequency. This is only an approximate correction, however, because the shift probably varies with frequency.

We now attempt to reanalyze DK's transmission measurements. We analyze only the thicker (4.2-mm) sample because it scattered less than did the 1.7-mm sample. (Their Fig. 3 is mislabeled: the 4.2-mm spectrum is actually the dashed line, not the solid line.) We compute the reflectivity of the interfaces for the system with and without sample. If the incident intensity at a particular wavelength is I_0 , the transmitted intensities through the sample I_S and through the blank I_B are given by Eqs. (3) and (4) [similar to DK's Eqs. (1) and (2)]:

$$I_S = (1 - r_K)^6 (1 - r_{KC})(1 - r_C) \exp(-k_{ext}d) I_0; \quad (3)$$

$$I_B = (1 - r_K)^6 I_0. \quad (4)$$

Here r_K is the Fresnel reflectivity of the window–vacuum interface using a KBr window, r_C is the reflectivity of the CO₂–vacuum interface, and r_{KC} is that of the window–CO₂ interface. The sample thickness is $d = 4.2$ mm, and the extinction coefficient k_{ext} (units of inverse length) is the sum of absorption and scattering coefficients:

$$k_{ext} = k_{scat} + k_{abs}. \quad (5)$$

Two KBr windows bounded the chamber, and the CO₂ was grown on a third window, accounting for the high powers of $(1 - r_K)$. DK plotted the transmittance t as a function of frequency ν defined as

$$t = I_S/I_B. \quad (6)$$

Putting Eqs. (3) and (4) into Eq. (6), we obtain

$$k_{ext}(\nu) = (-1/d) \ln \frac{t(\nu + 40)(1 - r_K)}{(1 - r_{KC})(1 - r_C)}, \quad (7)$$

where here we also apply the shift of 40 cm⁻¹ to the measured spectrum as discussed above.

The three reflectivities are obtained using the $m_{Re}(\lambda)$ of KBr from Fig. 8.14 of Ref. 38 and $m_{Re}(\lambda)$ of CO₂ from Wood and Roux.³¹ These values are ~1.5 and 1.4, respectively, with slight wavelength dependence. For $\lambda > 18$ μm Wood and Roux made no measurements on CO₂, so we assume $m_{Re} = 1.4$; this choice is confirmed by the KK analysis below.

Having thus obtained $k_{ext}(\lambda)$ from Eq. (7), we need to estimate $k_{scat}(\lambda)$ to obtain $k_{abs}(\lambda)$ from Eq. (5). The scattering coefficient k_{scat} is constrained as follows. We assume the Gaizauskas¹¹ values of k_{abs} in the 6–9-μm region (Fig. 9) to be correct, and we force the reanalysis of DK's results to agree with them as much as possible. DK's published m_{Im} exceeds that of Gaizauskas by a factor of 2 on average. DK's $m_{Im}(\lambda)$ also shows less structure suggesting that DK's spectral resolution was probably coarser than that of Gaizauskas. The $k_{scat}(\lambda)$ which causes DK's result to agree exactly with Gaizauskas is plotted as the solid line in Fig. 11

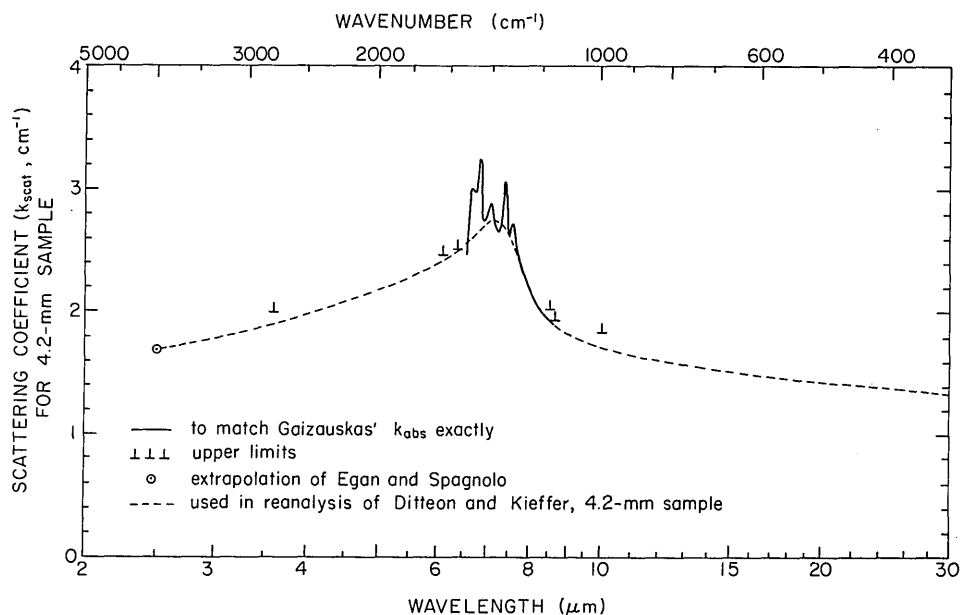


Fig. 11. Scattering coefficient k_{scat} for Ditteon and Kieffer's¹⁴ (DK's) cloudy sample, used for reanalysis of DK's transmission data resulting in the plots in Figs. 4, 9, and 10. DK's data have already been shifted in wave number by 40 cm^{-1} (see text) before deriving this $k_{\text{scat}}(\lambda)$. The solid line is the function $k_{\text{scat}}(\lambda)$, which, when subtracted from DK's observed extinction coefficient $k_{\text{ext}}(\lambda)$, results in an absorption coefficient $k_{\text{abs}}(\lambda)$ that agrees with values of Gaizauskas¹¹ (Fig. 9). The upper limit symbols at six wavelengths have their horizontal bases marking the values of k_{ext} at those wavelengths; k_{scat} cannot exceed k_{ext} because that would cause k_{abs} to be negative. The dashed line was used in the reanalysis of DK's transmission data.

with k_{scat} averaging $\sim 2.7 \text{ cm}^{-1}$. (DK thought that the scattering occurred predominantly at the rough surface rather than throughout the sample, but we can still mimic its effect here by use of a k_{scat} in units of inverse length because we are using data from only one sample of constant thickness.) Upper limits to k_{scat} can be obtained at other wavelengths by the criterion that k_{abs} cannot be negative, as shown in Fig. 11. The procedure for further constraining k_{scat} now becomes rather arbitrary. We postulate that the m_{Im} of Egan and Spagnolo in Fig. 4 can be extrapolated from 1.0 to $2.5 \mu\text{m}$ (except in the absorption lines measured by Fink and Sill) using the measured behavior of $m_{\text{Im}}(\lambda)$ from 0.6 to $1.0 \mu\text{m}$ as a guide. This gives a value of m_{Im} at $2.5 \mu\text{m}$ that implies $k_{\text{scat}} = 1.7 \text{ cm}^{-1}$. A smooth curve is then drawn (the dashed curve in Fig. 11) from this point, through the values implied by agreement with Gaizauskas at 6 – $9 \mu\text{m}$, obeying the strict upper limits provided. This causes k_{scat} to reach a maximum in the only region where its value is known, a disturbing coincidence. Such behavior may be justified by noting that (a) k_{scat} increased with time, and DK's spectrophotometer scanned from small to large wavelength; and (b) starting at a long wavelength, k_{scat} is expected to increase as the wavelength decreases until $\lambda \approx l$, where l is the length scale of the surface roughness features. This behavior of $k_{\text{scat}}(\lambda)$ may, therefore, be plausible if l is 5 – $10 \mu\text{m}$, but l was not measured by DK.

We take the dashed line in Fig. 11 as $k_{\text{scat}}(\lambda)$ and obtain $k_{\text{abs}}(\lambda)$ from Eq. (5). The corresponding m_{Im} is plotted in Figs. 4, 9, and 10 together with an upper limit to m_{Im} obtained by setting $k_{\text{scat}} = 0$. The relative uncertainty in the reevaluated m_{Im} is largest where

m_{Im} is very small. There is no constraint which gives a lower limit to m_{Im} in the regions near 3.6 , 6.2 , and $9.0 \mu\text{m}$, nor for $1.0 < \lambda < 2.5 \mu\text{m}$ and $\lambda \geq 20 \mu\text{m}$.

C. Compilation of Imaginary Index

Egan and Spagnolo's⁹ k_{abs} is approximately linear in $\log \lambda$ from 0.6 to $1.0 \mu\text{m}$. This dependence is extrapolated as a dashed line in Fig. 4 to match with reanalysis of DK at $\lambda = 2.5 \mu\text{m}$. The measurements by FS of the four absorption lines in this region (Fig. 5) are added.

In the 2.7 - μm band (Fig. 6) the results of WR are favored over those of FS because WR performed a KK analysis. We ignore WR where m_{Im} goes below 10^{-3} , because their samples were too thin to allow weak absorption to be measured accurately.

We interpolate between the reanalysis of DK at $2.60 \mu\text{m}$ and WR at $2.688 \mu\text{m}$, assuming $\log m_{\text{Im}}$ varies linearly with λ (Fig. 4). Similarly, $\log m_{\text{Im}}$ is interpolated linearly in λ from WR at $2.782 \mu\text{m}$ to DK-reanalyzed at $2.84 \mu\text{m}$. We ignore the curvature of DK's m_{Im} concave downward toward the band centers, both here and at 4.3 and $15 \mu\text{m}$, because it appears to be wrong when joined with the measurements by others at band center.

DK-reanalyzed is then used for 2.85 – $3.9 \mu\text{m}$ (Figs. 4 and 9); then $\log m_{\text{Im}}$ is interpolated linearly in λ to WR at $4.0 \mu\text{m}$. WR's measurements are used from 4.0 to $4.17 \mu\text{m}$ and from 4.4 to $4.5 \mu\text{m}$, but for the band center, 4.17 – $4.4 \mu\text{m}$ (Fig. 7), the reanalysis of YP is used. A smooth curve is drawn to interpolate from WR's data at $4.5 \mu\text{m}$ to DK-reanalyzed at $4.8 \mu\text{m}$.

A sharp absorption feature measured by FS at $4.9 \mu\text{m}$ (Fig. 9) exceeds the upper limit to m_{Im} from DK's measurements. We use DK-reanalyzed here, but note

that DK's spectrophotometer may not have resolved this peak sufficiently. Alternatively, perhaps this peak observed by FS at $4.9\ \mu\text{m}$ is the same one found by DK at $5.2\ \mu\text{m}$, which has been shifted to $5.1\ \mu\text{m}$ in the reanalysis. This interpretation would require that DK's wavelength calibration was much worse here than elsewhere in the IR.

We use DK-reanalyzed from 4.8 to $6.54\ \mu\text{m}$ (Fig. 9), then interpolate $\log m_{\text{Im}}$ vs λ to the Gaizauskas value at $6.64\ \mu\text{m}$. The Gaizauskas values are used from 6.64 to $8.76\ \mu\text{m}$. A smooth curve is drawn to connect the Gaizauskas value at $8.76\ \mu\text{m}$ to the DK-reanalyzed value at $9.0\ \mu\text{m}$. The reanalysis of DK's data is then used as far as $11.0\ \mu\text{m}$ (Fig. 10). We then interpolate $\log m_{\text{Im}}$ vs λ from $11.0\ \mu\text{m}$ to WR's value at $11.5\ \mu\text{m}$. WR's values are used from 11.5 to $13.9\ \mu\text{m}$, where they meet those of FS. FS's values are then used from 13.9 to $14.3\ \mu\text{m}$ and again from 16.0 to $16.2\ \mu\text{m}$.

For the band center, 14.3 – $16.0\ \mu\text{m}$, the transmission data of YP are reanalyzed in conjunction with the KK analysis of the entire spectrum, as described in Sec. VII.B, resulting in the solid line in Fig. 8.

From FS's value at $16.2\ \mu\text{m}$ a smooth curve is drawn to meet DK-reanalyzed at $17.9\ \mu\text{m}$ in Fig. 10. A gap in the compilation begins at $\lambda = 25\ \mu\text{m}$ because no measurements have been made at 25 – $80\text{-}\mu\text{m}$ wavelengths.

V. Far Infrared

There are two absorption lines in the far infrared due to lattice vibrations in the crystal^{39,40} at ~ 114 - and 68-cm^{-1} wave number (90 - and $150\text{-}\mu\text{m}$ wavelength). The absorption coefficient has been measured only in these lines, not in the regions of weak absorption outside the lines.

A. Sources of Data

Kuan³⁹ (1969) measured transmission through clear films of CO_2 ice of $20\text{-}\mu\text{m}$ thickness at several temperatures from 4.2 to $100\ \text{K}$ with spectral resolution of 0.3 – $0.5\ \text{cm}^{-1}$. Only the data for $4.2\ \text{K}$ were plotted in Kuan's thesis, but the linewidths, integrated strengths, and peak positions were tabulated at the higher temperatures. His sample thickness was given to only one significant figure, $0.02\ \text{mm}$, determined by measuring the thickness of the aluminum foil used for spacing the cell. His integrated intensities were "preliminary" because he did not account for reflection varying with wavelength across each peak. Kuan's plots of $\ln(I_B/I_S)$ vs ν at $4.2\ \text{K}$ are converted to m_{Im} (uncorrected for reflection) in Figs. 12 and 13 here. (We assume that the value of the top of the vertical axis in his Fig. 3 is wrong since it is inconsistent with the other marks on that axis.) Also plotted here are the adjusted values of m_{Im} at $100\ \text{K}$ using data from Kuan's Table I.

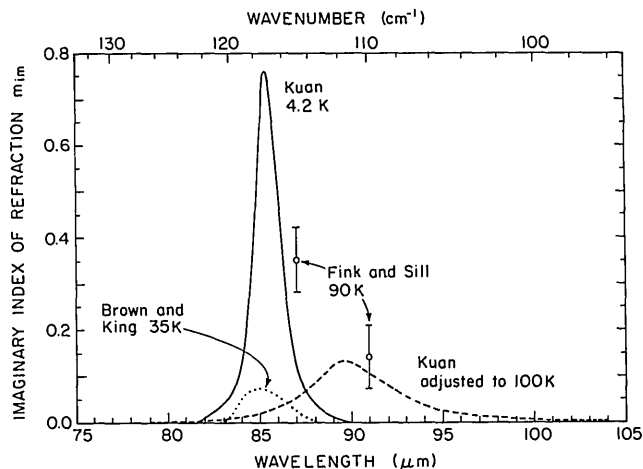


Fig. 12. Imaginary refractive index of CO_2 ice in the first far-IR absorption line.

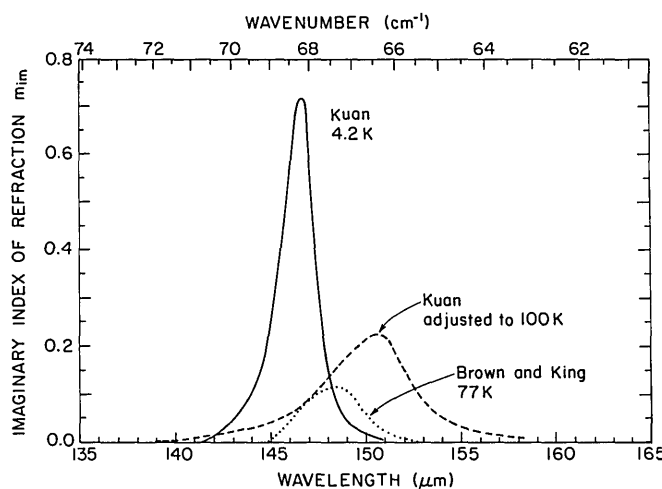


Fig. 13. Imaginary refractive index of CO_2 ice in the second far-IR absorption line.

Brown and King⁴⁰ (1970) (BK) grew thin films of unpurified CO_2 ice and measured transmission in the two absorption lines with 1.6-cm^{-1} resolution. They determined the sample thickness by measuring interference fringes at $\lambda = 21\ \mu\text{m}$ and assuming $m_{\text{Re}} = 1.51$ at that wavelength. Plots of $\ln(I_B/I_S)$ were given in their Figs. 1 and 2. (We assume that the value at the top of the vertical axis in their Fig. 2 is wrong because it is inconsistent with the other marks on that axis.) The corresponding values of m_{Im} are plotted here in Figs. 12 and 13. They are in gross disagreement with those of Kuan by factors of ~ 10 for the $90\text{-}\mu\text{m}$ line and 6 for the $105\text{-}\mu\text{m}$ line. BK's plot of their integrated absorption $\int \ln(I_B/I_S) d\nu$ vs film thickness (their Fig. 3) is also inconsistent with their own Figs. 1 and 2, suggesting

Table I. Real (m_{Re}) and imaginary (m_{Im}) parts of the complex index of refraction of CO_2 ice from 52-nm to 200-m wavelength (λ). Data sources and uncertainties are discussed in the text. These values are graphed as the solid lines in Figs. 14 and 15. Blanks appear in the table where no data are available; these regions correspond to the gaps in Fig. 14. Values of m_{Im} marked with asterisks are uncertain to more than an order of magnitude, as discussed in Secs. IV.B. and VII.C. Wavelengths were chosen for the tables to resolve adequately the variations in both real and imaginary indices. For intermediate wavelengths not given in the table, one should interpolate m_{Re} linearly in $\log \lambda$ and $\log m_{\text{Im}}$ linearly in $\log \lambda$. Table I is on pages 2663–2667.

$\lambda(\mu\text{m})$	m_{re}	m_{im}	$\lambda(\mu\text{m})$	m_{re}	m_{im}	$\lambda(\mu\text{m})$	m_{re}	m_{im}
5.2000E-2	0.509	1.16E-1	1.1770E-1	1.986	3.00E+0	1.4343E+0	1.401	5.50E-5
5.3000E-2	0.493	1.84E-1	1.1800E-1	2.240	3.01E+0	1.43440	1.401	1.16E-4
5.4100E-2	0.489	2.61E-1	1.1830E-1	2.501	2.99E+0	1.43446	1.401	1.40E-4
5.5100E-2	0.501	3.28E-1	1.1860E-1	2.778	2.94E+0	1.43451	1.401	1.50E-4
5.6400E-2	0.539	4.21E-1	1.1900E-1	3.157	2.80E+0	1.43454	1.401	1.46E-4
5.7400E-2	0.598	4.81E-1	1.1950E-1	3.627	2.47E+0	1.43460	1.401	1.24E-4
5.7900E-2	0.636	4.99E-1	1.2000E-1	3.855	1.83E+0	1.4347E+0	1.401	6.50E-5
5.8500E-2	0.682	5.13E-1	1.2050E-1	3.773	1.31E+0	1.4348E+0	1.401	3.75E-5
5.9000E-2	0.720	5.13E-1	1.2100E-1	3.609	1.02E+0	1.4349E+0	1.401	2.76E-5
5.9500E-2	0.752	5.12E-1	1.2150E-1	3.472	8.23E-1	1.4350E+0	1.401	2.17E-5
6.0200E-2	0.797	5.05E-1	1.2200E-1	3.352	6.59E-1	1.4352E+0	1.401	1.51E-5
6.2000E-2	0.869	4.48E-1	1.2250E-1	3.237	5.33E-1	1.4354E+0	1.401	1.03E-5
6.2600E-2	0.880	4.28E-1	1.2300E-1	3.134	4.36E-1	1.4356E+0	1.401	7.50E-6
6.3300E-2	0.884	4.09E-1	1.2400E-1	2.963	2.90E-1	1.4358E+0	1.401	5.70E-6
6.5300E-2	0.885	3.73E-1	1.2500E-1	2.818	1.69E-1	1.4359E+0	1.401	4.90E-6
6.7000E-2	0.870	3.52E-1	1.2600E-1	2.669	6.78E-2	1.4360E+0	1.401	4.44E-6
6.8500E-2	0.858	3.55E-1	1.2700E-1	2.516	9.68E-3	1.4361E+0	1.401	4.08E-6
7.0400E-2	0.830	3.34E-1	1.2750E-1	2.442		1.4362E+0	1.401	3.85E-6
7.2500E-2	0.790	3.66E-1	1.3000E-1	2.230		1.4363E+0	1.401	3.73E-6
7.4700E-2	0.748	3.88E-1	1.3300E-1	2.080		1.4364E+0	1.401	3.70E-6
7.7500E-2	0.704	4.90E-1	1.4000E-1	1.885		1.5000E+0	1.401	3.94E-6
7.9500E-2	0.705	5.78E-1	1.4400E-1	1.817		1.6000E+0	1.401	4.33E-6
8.0500E-2	0.727	6.33E-1	1.5000E-1	1.744		1.7000E+0	1.400	4.80E-6
8.1600E-2	0.765	6.65E-1	1.6000E-1	1.665		1.8000E+0	1.400	5.15E-6
8.2700E-2	0.805	6.97E-1	1.7000E-1	1.614		1.9000E+0	1.399	5.51E-6
8.3800E-2	0.848	7.06E-1	1.8000E-1	1.577		1.9582E+0	1.399	5.80E-6
8.4900E-2	0.901	7.21E-1	2.0000E-1	1.530		1.9584E+0	1.399	5.90E-6
8.6100E-2	0.944	6.68E-1	2.2000E-1	1.501		1.9588E+0	1.399	6.22E-6
8.7300E-2	0.931	6.17E-1	2.4000E-1	1.481		1.9592E+0	1.399	6.79E-6
8.7500E-2	0.922	6.10E-1	2.6000E-1	1.467		1.9596E+0	1.399	8.05E-6
8.8000E-2	0.898	6.02E-1	2.8000E-1	1.456		1.9600E+0	1.399	9.74E-6
8.8600E-2	0.860	6.02E-1	3.0000E-1	1.448		1.9610E+0	1.399	1.58E-5
8.9800E-2	0.817	6.75E-1	3.2000E-1	1.442		1.9620E+0	1.399	2.54E-5
9.1200E-2	0.820	7.52E-1	3.3300E-1	1.438	6.75E-7	1.9630E+0	1.398	4.20E-5
9.2500E-2	0.858	8.21E-1	3.6300E-1	1.432	6.78E-7	1.9636E+0	1.398	6.90E-5
9.3900E-2	0.910	8.49E-1	4.0100E-1	1.426	6.83E-7	1.9640E+0	1.398	1.05E-4
9.4500E-2	0.930	8.66E-1	4.2700E-1	1.423	6.94E-7	1.9646E+0	1.398	2.45E-4
9.5000E-2	0.952	8.78E-1	4.5200E-1	1.420	7.04E-7	1.9650E+0	1.398	6.80E-4
9.5400E-2	0.976	8.87E-1	4.9000E-1	1.417	7.37E-7	1.9652E+0	1.397	1.18E-3
9.6000E-2	1.012	8.79E-1	5.1500E-1	1.415	7.70E-7	1.9654E+0	1.398	1.72E-3
9.6500E-2	1.035	8.63E-1	5.5300E-1	1.413	8.27E-7	1.9656E+0	1.398	2.29E-3
9.6900E-2	1.044	8.43E-1	5.7800E-1	1.412	8.91E-7	1.9658E+0	1.399	2.51E-3
9.7500E-2	1.044	8.22E-1	6.1600E-1	1.411	9.92E-7	1.9659E+0	1.399	2.50E-3
9.8000E-2	1.034	8.08E-1	6.7900E-1	1.409	1.17E-6	1.9660E+0	1.400	2.36E-3
9.8400E-2	1.025	8.09E-1	7.4200E-1	1.407	1.36E-6	1.9661E+0	1.400	2.00E-3
9.9000E-2	1.016	8.09E-1	8.0500E-1	1.406	1.55E-6	1.9662E+0	1.400	1.55E-3
9.9500E-2	1.008	8.11E-1	8.6800E-1	1.406	1.73E-6	1.9664E+0	1.400	8.50E-4
1.0000E-1	0.996	8.13E-1	9.3100E-1	1.405	1.92E-6	1.9666E+0	1.400	2.75E-4
1.0160E-1	0.966	8.58E-1	1.0000E+0	1.404	2.13E-6	1.9668E+0	1.400	1.61E-4
1.0330E-1	0.952	9.30E-1	1.1000E+0	1.403	2.50E-6	1.9670E+0	1.400	1.12E-4
1.0510E-1	0.975	1.03E+0	1.2000E+0	1.403	2.86E-6	1.9674E+0	1.400	6.35E-5
1.0690E-1	1.040	1.10E+0	1.3000E+0	1.402	3.24E-6	1.9680E+0	1.399	3.07E-5
1.0900E-1	1.079	1.11E+0	1.4000E+0	1.401	3.60E-6	1.9684E+0	1.399	2.17E-5
1.1100E-1	1.039	1.16E+0	1.4325E+0	1.401	3.70E-6	1.9690E+0	1.399	1.44E-5
1.1200E-1	0.981	1.22E+0	1.4327E+0	1.401	3.76E-6	1.9700E+0	1.399	8.65E-6
1.1300E-1	0.894	1.33E+0	1.4328E+0	1.401	3.86E-6	1.9706E+0	1.399	6.60E-6
1.1400E-1	0.818	1.56E+0	1.4330E+0	1.401	4.25E-6	1.9708E+0	1.399	6.20E-6
1.1500E-1	0.817	1.89E+0	1.4332E+0	1.401	5.25E-6	1.9710E+0	1.399	5.98E-6
1.1550E-1	0.866	2.11E+0	1.4335E+0	1.401	8.25E-6	1.9713E+0	1.399	5.80E-6
1.1600E-1	0.979	2.34E+0	1.4338E+0	1.401	1.44E-5	2.0045E+0	1.398	5.90E-6
1.1650E-1	1.161	2.59E+0	1.4340E+0	1.401	2.22E-5	2.0050E+0	1.398	6.20E-6
1.1700E-1	1.435	2.82E+0	1.4341E+0	1.401	2.77E-5	2.0054E+0	1.398	6.65E-6
1.1730E-1	1.659	2.93E+0	1.4342E+0	1.401	3.64E-5	2.0060E+0	1.398	8.95E-6

$\lambda(\mu\text{m})$	m_{re}	m_{im}	$\lambda(\mu\text{m})$	m_{re}	m_{im}	$\lambda(\mu\text{m})$	m_{re}	m_{im}
2.0070E+0	1.398	1.57E-5	2.6000E+0	1.394	5.50E-5	2.8400E+0	1.395	9.60E-5
2.0080E+0	1.398	3.00E-5	2.6200E+0	1.393	1.25E-4	2.8600E+0	1.394	5.50E-5
2.0090E+0	1.398	7.30E-5	2.6400E+0	1.393	2.78E-4	2.8700E+0	1.394	4.30E-5
2.0100E+0	1.398	2.32E-4	2.6600E+0	1.392	6.25E-4	2.8800E+0	1.394	3.95E-5
2.0110E+0	1.397	8.45E-4	2.6750E+0	1.390	1.14E-3	2.8900E+0	1.394	3.85E-5
2.0113E+0	1.397	2.15E-3	2.6800E+0	1.389	1.42E-3	2.9000E+0	1.394	3.86E-5
2.0116E+0	1.398	3.75E-3	2.6820E+0	1.388	1.60E-3	2.9100E+0	1.393	4.02E-5
2.0117E+0	1.398	3.95E-3	2.6840E+0	1.387	1.82E-3	2.9300E+0	1.393	4.40E-5
2.0118E+0	1.400	3.89E-3	2.6860E+0	1.385	2.28E-3	2.9600E+0	1.393	5.30E-5
2.0119E+0	1.400	3.35E-3	2.6870E+0	1.384	2.70E-3	3.0000E+0	1.392	7.10E-5
2.0120E+0	1.401	2.40E-3	2.6880E+0	1.382	3.80E-3	3.0200E+0	1.392	7.95E-5
2.0121E+0	1.401	1.50E-3	2.6900E+0	1.378	9.40E-3	3.0400E+0	1.391	8.41E-5
2.0123E+0	1.400	8.50E-4	2.6920E+0	1.380	2.00E-2	3.0700E+0	1.391	8.70E-5
2.0125E+0	1.400	5.75E-4	2.6940E+0	1.390	2.80E-2	3.0900E+0	1.391	8.75E-5
2.0130E+0	1.400	2.32E-4	2.6950E+0	1.398	2.75E-2	3.1000E+0	1.390	8.70E-5
2.0135E+0	1.400	9.10E-5	2.6960E+0	1.404	2.35E-2	3.1100E+0	1.390	8.65E-5
2.0140E+0	1.399	4.10E-5	2.6980E+0	1.408	1.40E-2	3.1200E+0	1.390	8.17E-5
2.0145E+0	1.399	2.25E-5	2.7030E+0	1.403	3.00E-3	3.1500E+0	1.390	6.75E-5
2.0150E+0	1.399	1.50E-5	2.7060E+0	1.401	1.36E-3	3.1800E+0	1.389	5.45E-5
2.0155E+0	1.399	9.62E-6	2.7080E+0	1.399	8.60E-4	3.2100E+0	1.389	4.50E-5
2.0160E+0	1.399	7.60E-6	2.7090E+0	1.399	7.50E-4	3.2500E+0	1.388	3.46E-5
2.0165E+0	1.399	6.65E-6	2.7100E+0	1.398	7.00E-4	3.2600E+0	1.387	3.34E-5
2.0170E+0	1.399	6.20E-6	2.7110E+0	1.398	6.80E-4	3.2700E+0	1.387	3.22E-5
2.0175E+0	1.399	5.90E-6	2.7120E+0	1.398	6.70E-4	3.2800E+0	1.387	3.35E-5
2.0646E+0	1.398	6.10E-6	2.7130E+0	1.397	6.80E-4	3.2900E+0	1.387	3.80E-5
2.0650E+0	1.398	6.25E-6	2.7140E+0	1.397	7.10E-4	3.3000E+0	1.386	4.65E-5
2.0654E+0	1.398	6.55E-6	2.7160E+0	1.396	8.90E-4	3.3100E+0	1.386	5.90E-5
2.0660E+0	1.398	7.35E-6	2.7170E+0	1.396	1.00E-3	3.3200E+0	1.386	4.90E-5
2.0666E+0	1.398	8.75E-6	2.7180E+0	1.396	1.12E-3	3.3300E+0	1.386	3.75E-5
2.0670E+0	1.398	1.00E-5	2.7200E+0	1.396	1.22E-3	3.3400E+0	1.386	2.95E-5
2.0676E+0	1.398	1.35E-5	2.7240E+0	1.395	1.33E-3	3.3500E+0	1.385	2.55E-5
2.0680E+0	1.398	1.95E-5	2.7280E+0	1.395	1.41E-3	3.4000E+0	1.384	1.55E-5
2.0684E+0	1.398	3.35E-5	2.7340E+0	1.395	1.45E-3	3.4500E+0	1.383	9.85E-6**
2.0688E+0	1.398	1.36E-4	2.7400E+0	1.394	1.52E-3	3.5000E+0	1.381	6.20E-6**
2.0690E+0	1.398	2.95E-4	2.7460E+0	1.394	1.58E-3	3.5500E+0	1.379	4.05E-6**
2.0692E+0	1.398	5.50E-4	2.7500E+0	1.394	1.65E-3	3.6000E+0	1.377	2.67E-6**
2.0694E+0	1.398	8.30E-4	2.7540E+0	1.393	1.75E-3	3.6400E+0	1.375	2.39E-6**
2.0695E+0	1.398	8.70E-4	2.7580E+0	1.393	1.93E-3	3.6700E+0	1.373	2.36E-6**
2.0696E+0	1.398	8.50E-4	2.7600E+0	1.393	2.07E-3	3.6900E+0	1.372	2.39E-6**
2.0697E+0	1.399	7.60E-4	2.7620E+0	1.392	2.32E-3	3.7200E+0	1.370	2.50E-6**
2.0698E+0	1.399	6.30E-4	2.7640E+0	1.392	2.69E-3	3.7400E+0	1.368	2.68E-6**
2.0700E+0	1.399	3.25E-4	2.7660E+0	1.392	3.07E-3	3.7600E+0	1.367	3.05E-6**
2.0702E+0	1.399	1.40E-4	2.7680E+0	1.391	3.54E-3	3.7800E+0	1.365	3.70E-6**
2.0706E+0	1.399	4.72E-5	2.7700E+0	1.391	4.08E-3	3.8000E+0	1.363	6.60E-6**
2.0710E+0	1.399	2.36E-5	2.7720E+0	1.390	4.75E-3	3.8400E+0	1.358	2.20E-5
2.0714E+0	1.398	1.56E-5	2.7730E+0	1.389	5.10E-3	3.8700E+0	1.355	5.20E-5
2.0720E+0	1.398	1.10E-5	2.7740E+0	1.387	5.90E-3	3.9000E+0	1.350	9.90E-5
2.0730E+0	1.398	8.00E-6	2.7750E+0	1.385	8.50E-3	4.0000E+0	1.326	1.68E-3
2.0740E+0	1.398	6.40E-6	2.7760E+0	1.383	1.72E-2	4.0100E+0	1.322	2.04E-3
2.0744E+0	1.398	6.10E-6	2.7768E+0	1.389	2.50E-2	4.0200E+0	1.318	2.56E-3
2.1000E+0	1.398	6.18E-6	2.7773E+0	1.395	2.61E-2	4.0300E+0	1.313	3.44E-3
2.2000E+0	1.398	6.62E-6	2.7780E+0	1.404	2.53E-2	4.0400E+0	1.307	5.93E-3
2.3000E+0	1.397	7.08E-6	2.7790E+0	1.410	1.40E-2	4.0500E+0	1.302	1.13E-2
2.4000E+0	1.396	7.60E-6	2.7810E+0	1.407	4.80E-3	4.0600E+0	1.300	1.58E-2
2.4700E+0	1.396	8.08E-6	2.7820E+0	1.405	2.86E-3	4.0650E+0	1.300	1.84E-2
2.4900E+0	1.395	8.36E-6	2.7840E+0	1.402	1.07E-3	4.0680E+0	1.301	1.94E-2
2.5100E+0	1.395	8.88E-6	2.7850E+0	1.401	7.50E-4	4.0720E+0	1.302	1.93E-2
2.5300E+0	1.395	9.75E-6	2.7860E+0	1.401	6.25E-4	4.0750E+0	1.303	1.83E-2
2.5500E+0	1.395	1.09E-5	2.7880E+0	1.400	4.95E-4	4.0800E+0	1.301	1.61E-2
2.5600E+0	1.395	1.25E-5	2.7900E+0	1.399	4.29E-4	4.0850E+0	1.300	1.51E-2
2.5700E+0	1.395	1.53E-5	2.7920E+0	1.398	3.87E-4	4.0900E+0	1.298	1.38E-2
2.5800E+0	1.394	2.35E-5	2.7940E+0	1.398	3.54E-4	4.0950E+0	1.295	1.08E-2
2.5900E+0	1.394	3.75E-5	2.7960E+0	1.398	3.32E-4	4.0980E+0	1.292	9.30E-3

$\lambda(\mu\text{m})$	m_{re}	m_{im}	$\lambda(\mu\text{m})$	m_{re}	m_{im}	$\lambda(\mu\text{m})$	m_{re}	m_{im}
4.1000E+0	1.290	8.90E-3	4.3450E+0	1.661	1.23E-2	5.1100E+0	1.431	1.20E-4
4.1050E+0	1.286	8.50E-3	4.3500E+0	1.641	1.07E-2	5.1200E+0	1.431	6.50E-5
4.1100E+0	1.281	8.30E-3	4.3550E+0	1.622	1.05E-2	5.1300E+0	1.431	3.55E-5
4.1200E+0	1.271	8.20E-3	4.3600E+0	1.606	1.14E-2	5.1400E+0	1.430	4.30E-5
4.1250E+0	1.266	8.42E-3	4.3650E+0	1.590	1.36E-2	5.1500E+0	1.430	5.00E-5
4.1300E+0	1.260	7.70E-3	4.3700E+0	1.574	1.88E-2	5.1600E+0	1.430	4.30E-5
4.1330E+0	1.256	7.35E-3	4.3750E+0	1.559	2.84E-2	5.1800E+0	1.429	3.00E-5
4.1350E+0	1.253	7.40E-3	4.3800E+0	1.552	5.52E-2	5.2000E+0	1.429	2.65E-5
4.1400E+0	1.246	7.90E-3	4.3840E+0	1.567	7.53E-2	5.2400E+0	1.428	2.05E-5
4.1450E+0	1.237	8.75E-3	4.3860E+0	1.584	7.83E-2	5.2800E+0	1.427	1.66E-5
4.1500E+0	1.229	1.07E-2	4.3880E+0	1.601	6.99E-2	5.3200E+0	1.426	1.41E-5
4.1530E+0	1.225	1.19E-2	4.3900E+0	1.611	5.50E-2	5.4000E+0	1.425	1.09E-5
4.1550E+0	1.222	1.18E-2	4.3980E+0	1.591	1.11E-2	5.5000E+0	1.423	8.05E-6**
4.1600E+0	1.213	1.08E-2	4.4000E+0	1.582	6.80E-3	5.6000E+0	1.422	6.20E-6**
4.1650E+0	1.200	1.01E-2	4.4050E+0	1.569	7.75E-3	5.7000E+0	1.420	5.05E-6**
4.1800E+0	1.150	1.85E-2	4.4100E+0	1.561	7.82E-3	5.8000E+0	1.419	4.15E-6**
4.1900E+0	1.108	4.76E-2	4.4150E+0	1.555	6.55E-3	5.9000E+0	1.419	3.63E-6**
4.2000E+0	1.074	7.70E-2	4.4200E+0	1.549	4.80E-3	6.0000E+0	1.418	3.23E-6**
4.2100E+0	1.037	1.19E-1	4.4220E+0	1.546	4.50E-3	6.1000E+0	1.417	3.04E-6**
4.2200E+0	0.999	1.63E-1	4.4250E+0	1.542	4.55E-3	6.2000E+0	1.416	2.95E-6**
4.2300E+0	0.951	2.23E-1	4.4400E+0	1.529	4.92E-3	6.3000E+0	1.416	3.07E-6**
4.2350E+0	0.920	2.55E-1	4.4550E+0	1.519	5.25E-3	6.3500E+0	1.415	3.28E-6**
4.2400E+0	0.882	2.99E-1	4.4600E+0	1.516	5.31E-3	6.4000E+0	1.415	3.66E-6**
4.2450E+0	0.831	3.42E-1	4.4650E+0	1.514	5.08E-3	6.4400E+0	1.415	4.10E-6**
4.2500E+0	0.733	3.94E-1	4.4700E+0	1.512	4.65E-3	6.4600E+0	1.415	4.40E-6**
4.2520E+0	0.669	4.49E-1	4.4750E+0	1.510	3.90E-3	6.5000E+0	1.414	6.30E-6**
4.2540E+0	0.605	5.20E-1	4.4800E+0	1.508	3.05E-3	6.5200E+0	1.414	7.80E-6**
4.2560E+0	0.551	6.32E-1	4.4840E+0	1.506	2.44E-3	6.6400E+0	1.414	2.48E-5
4.2580E+0	0.509	7.38E-1	4.4880E+0	1.504	1.87E-3	6.6520E+0	1.414	2.86E-5
4.2600E+0	0.466	8.86E-1	4.4900E+0	1.503	1.69E-3	6.6680E+0	1.414	3.49E-5
4.2620E+0	0.444	1.07E+0	4.4920E+0	1.502	1.56E-3	6.6830E+0	1.414	4.00E-5
4.2640E+0	0.457	1.29E+0	4.4960E+0	1.500	1.38E-3	6.6980E+0	1.413	4.93E-5
4.2660E+0	0.516	1.54E+0	4.5000E+0	1.498	1.26E-3	6.7140E+0	1.413	5.95E-5
4.2670E+0	0.558	1.67E+0	4.5200E+0	1.490	9.70E-4	6.7290E+0	1.413	7.23E-5
4.2680E+0	0.610	1.84E+0	4.5600E+0	1.478	6.10E-4	6.7450E+0	1.413	8.17E-5
4.2690E+0	0.706	2.06E+0	4.6000E+0	1.469	4.10E-4	6.7600E+0	1.413	8.78E-5
4.2700E+0	0.888	2.28E+0	4.6400E+0	1.462	3.05E-4	6.7760E+0	1.413	9.19E-5
4.2710E+0	1.151	2.47E+0	4.6800E+0	1.457	2.34E-4	6.7920E+0	1.413	9.42E-5
4.2720E+0	1.507	2.63E+0	4.7200E+0	1.453	1.91E-4	6.8080E+0	1.413	9.53E-5
4.2730E+0	1.960	2.67E+0	4.7600E+0	1.449	1.44E-4	6.8240E+0	1.413	9.42E-5
4.2740E+0	2.413	2.50E+0	4.8000E+0	1.446	1.03E-4	6.8400E+0	1.413	9.40E-5
4.2750E+0	2.764	2.20E+0	4.8200E+0	1.444	8.00E-5	6.8560E+0	1.413	9.76E-5
4.2760E+0	2.967	1.81E+0	4.8300E+0	1.443	6.60E-5	6.9040E+0	1.413	1.14E-4
4.2770E+0	3.051	1.46E+0	4.8400E+0	1.443	6.36E-5	6.9210E+0	1.413	1.17E-4
4.2780E+0	2.995	1.08E+0	4.8500E+0	1.442	6.50E-5	6.9370E+0	1.413	1.18E-4
4.2790E+0	2.866	8.68E-1	4.8600E+0	1.441	7.40E-5	6.9540E+0	1.413	1.14E-4
4.2800E+0	2.746	7.19E-1	4.8750E+0	1.441	9.20E-5	6.9870E+0	1.412	9.17E-5
4.2810E+0	2.634	6.20E-1	4.8800E+0	1.440	8.60E-5	7.0210E+0	1.412	7.15E-5
4.2820E+0	2.544	5.62E-1	4.9000E+0	1.439	5.50E-5	7.0550E+0	1.412	5.51E-5
4.2840E+0	2.422	4.74E-1	4.9200E+0	1.438	4.75E-5	7.0890E+0	1.412	4.65E-5
4.2860E+0	2.336	4.10E-1	4.9400E+0	1.437	4.30E-5	7.1230E+0	1.412	4.05E-5
4.2880E+0	2.271	3.54E-1	4.9500E+0	1.437	4.12E-5	7.1410E+0	1.412	3.93E-5
4.2900E+0	2.212	3.01E-1	4.9600E+0	1.436	4.14E-5	7.1580E+0	1.412	3.93E-5
4.2950E+0	2.100	2.21E-1	4.9750E+0	1.436	4.35E-5	7.1760E+0	1.411	4.04E-5
4.3000E+0	2.008	1.48E-1	4.9800E+0	1.436	4.32E-5	7.1940E+0	1.411	4.27E-5
4.3050E+0	1.930	1.14E-1	5.0000E+0	1.435	4.15E-5	7.2290E+0	1.411	5.06E-5
4.3100E+0	1.872	9.18E-2	5.0200E+0	1.434	3.40E-5	7.2650E+0	1.411	5.86E-5
4.3150E+0	1.828	7.49E-2	5.0300E+0	1.434	3.05E-5	7.2840E+0	1.411	6.19E-5
4.3200E+0	1.793	6.13E-2	5.0400E+0	1.433	2.93E-5	7.3020E+0	1.411	6.38E-5
4.3250E+0	1.763	4.77E-2	5.0500E+0	1.433	2.95E-5	7.3380E+0	1.411	6.56E-5
4.3300E+0	1.736	3.56E-2	5.0600E+0	1.432	4.50E-5	7.3760E+0	1.411	6.80E-5
4.3350E+0	1.710	2.39E-2	5.0900E+0	1.432	1.60E-4	7.3940E+0	1.411	7.21E-5
4.3400E+0	1.684	1.60E-2	5.1000E+0	1.431	1.95E-4	7.4130E+0	1.411	7.92E-5

$\lambda(\mu\text{m})$	m_{re}	m_{im}	$\lambda(\mu\text{m})$	m_{re}	m_{im}	$\lambda(\mu\text{m})$	m_{re}	m_{im}
7.4510E+0	1.410	9.97E-5	1.0500E+1	1.398	1.85E-5	1.5147E+1	0.750	1.74E+0
7.4890E+0	1.410	1.16E-4	1.0600E+1	1.397	2.05E-5	1.5150E+1	0.915	1.78E+0
7.5080E+0	1.410	1.21E-4	1.0700E+1	1.396	2.42E-5	1.5152E+1	1.017	1.78E+0
7.5280E+0	1.410	1.20E-4	1.0800E+1	1.395	3.50E-5	1.5155E+1	1.163	1.79E+0
7.5470E+0	1.410	1.15E-4	1.0900E+1	1.395	5.00E-5	1.5160E+1	1.391	1.74E+0
7.5670E+0	1.410	1.04E-4	1.1000E+1	1.394	8.00E-5	1.5165E+1	1.592	1.65E+0
7.6060E+0	1.410	8.40E-5	1.1500E+1	1.386	3.00E-3	1.5170E+1	1.763	1.52E+0
7.6460E+0	1.410	6.92E-5	1.1630E+1	1.385	6.40E-3	1.5175E+1	1.884	1.35E+0
7.6660E+0	1.410	6.52E-5	1.1700E+1	1.386	7.90E-3	1.5180E+1	1.950	1.18E+0
7.7070E+0	1.410	6.38E-5	1.1760E+1	1.388	8.50E-3	1.5185E+1	1.983	1.02E+0
7.7270E+0	1.410	6.23E-5	1.1800E+1	1.388	8.40E-3	1.5190E+1	1.975	8.47E-1
7.7680E+0	1.409	5.38E-5	1.1900E+1	1.389	6.80E-3	1.5195E+1	1.926	7.06E-1
7.8100E+0	1.409	4.68E-5	1.2050E+1	1.388	4.40E-3	1.5200E+1	1.849	5.86E-1
7.8520E+0	1.409	3.97E-5	1.2200E+1	1.385	4.60E-3	1.5205E+1	1.750	5.02E-1
7.8940E+0	1.409	3.28E-5	1.2350E+1	1.383	4.80E-3	1.5210E+1	1.645	4.57E-1
7.9370E+0	1.409	2.75E-5	1.2500E+1	1.381	4.80E-3	1.5215E+1	1.547	4.42E-1
7.9590E+0	1.409	2.54E-5	1.2660E+1	1.377	4.70E-3	1.5220E+1	1.460	4.45E-1
7.9810E+0	1.409	2.47E-5	1.2820E+1	1.373	7.90E-3	1.5222E+1	1.427	4.52E-1
8.0030E+0	1.409	2.45E-5	1.2990E+1	1.372	1.14E-2	1.5225E+1	1.383	4.62E-1
8.0250E+0	1.408	2.49E-5	1.3000E+1	1.372	1.18E-2	1.5230E+1	1.312	4.84E-1
8.0470E+0	1.408	2.54E-5	1.3080E+1	1.372	1.25E-2	1.5235E+1	1.243	5.12E-1
8.0690E+0	1.408	2.78E-5	1.3160E+1	1.373	1.25E-2	1.5240E+1	1.172	5.46E-1
8.1140E+0	1.408	3.32E-5	1.3200E+1	1.373	1.19E-2	1.5245E+1	1.087	5.88E-1
8.1590E+0	1.408	3.83E-5	1.3330E+1	1.371	9.30E-3	1.5250E+1	0.993	6.66E-1
8.1820E+0	1.408	3.88E-5	1.3510E+1	1.366	6.70E-3	1.5255E+1	0.902	7.72E-1
8.2050E+0	1.408	3.74E-5	1.3700E+1	1.358	5.30E-3	1.5257E+1	0.855	8.12E-1
8.2280E+0	1.408	3.54E-5	1.3800E+1	1.353	4.25E-3	1.5260E+1	0.778	9.26E-1
8.2750E+0	1.408	3.05E-5	1.3900E+1	1.347	3.45E-3	1.5262E+1	0.741	1.03E+0
8.2990E+0	1.408	2.80E-5	1.3950E+1	1.343	3.00E-3	1.5265E+1	0.721	1.20E+0
8.3220E+0	1.407	2.62E-5	1.4000E+1	1.339	2.40E-3	1.5267E+1	0.738	1.33E+0
8.3460E+0	1.407	2.60E-5	1.4060E+1	1.334	2.20E-3	1.5270E+1	0.809	1.50E+0
8.3940E+0	1.407	2.61E-5	1.4100E+1	1.330	2.25E-3	1.5275E+1	0.964	1.74E+0
8.4430E+0	1.407	2.06E-5	1.4200E+1	1.319	2.75E-3	1.5280E+1	1.170	1.95E+0
8.4920E+0	1.407	1.54E-5	1.4300E+1	1.307	3.56E-3	1.5284E+1	1.391	2.11E+0
8.5420E+0	1.407	1.15E-5	1.4400E+1	1.291	4.81E-3	1.5286E+1	1.528	2.17E+0
8.6000E+0	1.407	9.70E-6**	1.4500E+1	1.271	6.79E-3	1.5288E+1	1.677	2.21E+0
8.6500E+0	1.406	7.75E-6**	1.4600E+1	1.245	9.80E-3	1.5290E+1	1.833	2.23E+0
8.7000E+0	1.406	6.25E-6**	1.4700E+1	1.207	1.48E-2	1.5292E+1	1.992	2.24E+0
8.7500E+0	1.406	5.10E-6**	1.4800E+1	1.148	2.53E-2	1.5295E+1	2.228	2.21E+0
8.7600E+0	1.406	4.80E-6**	1.4900E+1	1.050	6.35E-2	1.5297E+1	2.391	2.17E+0
8.8000E+0	1.406	4.32E-6**	1.4950E+1	0.981	1.08E-1	1.5300E+1	2.633	2.08E+0
8.8400E+0	1.406	3.92E-6**	1.5000E+1	0.905	1.84E-1	1.5302E+1	2.788	1.97E+0
8.8800E+0	1.406	3.70E-6**	1.5020E+1	0.875	2.20E-1	1.5305E+1	2.981	1.78E+0
8.9200E+0	1.405	3.56E-6**	1.5040E+1	0.836	2.51E-1	1.5310E+1	3.171	1.39E+0
8.9400E+0	1.405	3.53E-6**	1.5060E+1	0.780	2.94E-1	1.5315E+1	3.232	1.01E+0
8.9600E+0	1.405	3.56E-6**	1.5070E+1	0.738	3.11E-1	1.5318E+1	3.217	7.76E-1
9.0000E+0	1.405	3.63E-6**	1.5080E+1	0.673	3.41E-1	1.5320E+1	3.173	6.26E-1
9.1000E+0	1.405	3.80E-6**	1.5090E+1	0.602	4.15E-1	1.5325E+1	2.974	3.57E-1
9.2000E+0	1.404	4.60E-6**	1.5100E+1	0.536	5.01E-1	1.5327E+1	2.888	2.96E-1
9.4000E+0	1.403	7.70E-6**	1.5105E+1	0.500	5.55E-1	1.5330E+1	2.770	2.34E-1
9.6000E+0	1.403	1.20E-5**	1.5110E+1	0.465	6.18E-1	1.5340E+1	2.522	1.57E-1
9.6300E+0	1.402	1.22E-5**	1.5112E+1	0.446	6.39E-1	1.5350E+1	2.365	1.08E-1
9.6600E+0	1.402	1.20E-5**	1.5115E+1	0.411	6.92E-1	1.5360E+1	2.253	8.60E-2
9.7000E+0	1.402	1.07E-5**	1.5117E+1	0.391	7.36E-1	1.5380E+1	2.102	5.53E-2
9.7500E+0	1.402	8.00E-6**	1.5120E+1	0.371	8.13E-1	1.5400E+1	1.998	3.85E-2
9.8000E+0	1.402	7.70E-6**	1.5122E+1	0.366	8.64E-1	1.5420E+1	1.922	3.10E-2
9.8800E+0	1.401	7.45E-6**	1.5125E+1	0.364	9.44E-1	1.5440E+1	1.865	2.72E-2
9.9000E+0	1.401	7.50E-6**	1.5130E+1	0.368	1.08E+0	1.5460E+1	1.819	2.48E-2
1.0000E+1	1.401	7.90E-6**	1.5135E+1	0.390	1.24E+0	1.5480E+1	1.782	2.36E-2
1.0100E+1	1.400	8.70E-6**	1.5137E+1	0.404	1.31E+0	1.5500E+1	1.750	2.30E-2
1.0200E+1	1.400	1.04E-5	1.5140E+1	0.447	1.45E+0	1.5520E+1	1.723	2.32E-2
1.0300E+1	1.399	1.20E-5	1.5142E+1	0.498	1.54E+0	1.5540E+1	1.699	2.44E-2
1.0400E+1	1.398	1.54E-5	1.5145E+1	0.628	1.69E+0	1.5560E+1	1.676	2.62E-2

$\lambda(\mu\text{m})$	m_{re}	m_{im}	$\lambda(\mu\text{m})$	m_{re}	m_{im}	$\lambda(\mu\text{m})$	m_{re}	m_{im}
1.5580E+1	1.655	2.94E-2	6.6000E+1	1.419		1.2600E+2	1.423	
1.5600E+1	1.632	3.50E-2	6.8000E+1	1.417		1.2800E+2	1.421	
1.5610E+1	1.619	4.29E-2	7.0000E+1	1.416		1.3000E+2	1.419	
1.5620E+1	1.609	5.42E-2	7.2000E+1	1.414		1.3200E+2	1.416	
1.5626E+1	1.603	6.28E-2	7.3000E+1	1.413		1.3400E+2	1.412	
1.5634E+1	1.600	8.13E-2	7.4000E+1	1.412		1.3600E+2	1.407	
1.5642E+1	1.606	9.79E-2	7.5000E+1	1.411		1.3650E+2	1.405	
1.5650E+1	1.620	1.11E-1	7.6000E+1	1.410		1.3700E+2	1.403	
1.5660E+1	1.641	1.14E-1	7.7000E+1	1.408		1.3800E+2	1.399	
1.5666E+1	1.655	1.11E-1	7.7500E+1	1.407		1.3896E+2	1.394	
1.5675E+1	1.670	9.83E-2	7.8000E+1	1.406		1.3986E+2	1.388	3.50E-3
1.5680E+1	1.675	8.62E-2	7.8500E+1	1.404		1.4079E+2	1.382	7.80E-3
1.5690E+1	1.674	6.63E-2	7.9000E+1	1.403		1.4235E+2	1.371	1.64E-2
1.5700E+1	1.666	5.27E-2	7.9500E+1	1.401		1.4330E+2	1.365	2.36E-2
1.5710E+1	1.659	4.60E-2	7.9800E+1	1.400		1.4425E+2	1.358	3.09E-2
1.5720E+1	1.652	4.06E-2	8.0160E+1	1.398		1.4524E+2	1.347	4.30E-2
1.5740E+1	1.641	3.48E-2	8.0790E+1	1.396	3.00E-3	1.4623E+2	1.336	6.29E-2
1.5760E+1	1.631	2.90E-2	8.2070E+1	1.392	5.50E-3	1.4670E+2	1.331	7.75E-2
1.5800E+1	1.614	2.28E-2	8.3400E+1	1.385	8.40E-3	1.4724E+2	1.329	9.73E-2
1.5850E+1	1.598	1.84E-2	8.4760E+1	1.374	1.61E-2	1.4770E+2	1.331	1.16E-1
1.5900E+1	1.584	1.55E-2	8.5440E+1	1.367	2.30E-2	1.4827E+2	1.337	1.42E-1
1.6000E+1	1.563	1.18E-2	8.6150E+1	1.361	3.36E-2	1.4870E+2	1.349	1.65E-1
1.6100E+1	1.547	9.00E-3	8.6880E+1	1.356	4.88E-2	1.4929E+2	1.374	1.88E-1
1.6200E+1	1.535	7.00E-3	8.7640E+1	1.354	7.06E-2	1.4970E+2	1.395	2.03E-1
1.6400E+1	1.515	5.20E-3	8.8000E+1	1.357	8.40E-2	1.5000E+2	1.414	2.12E-1
1.6700E+1	1.497	3.75E-3	8.8370E+1	1.362	9.81E-2	1.5034E+2	1.440	2.19E-1
1.7000E+1	1.485	2.72E-3	8.8840E+1	1.377	1.19E-1	1.5068E+2	1.467	2.21E-1
1.7400E+1	1.474	1.76E-3	8.9120E+1	1.392	1.27E-1	1.5105E+2	1.501	2.19E-1
1.7700E+1	1.468	1.34E-3	8.9280E+1	1.401	1.29E-1	1.5140E+2	1.534	2.02E-1
1.8000E+1	1.463	1.02E-3	8.9440E+1	1.410	1.30E-1	1.5177E+2	1.558	1.75E-1
1.8400E+1	1.458	7.25E-4	8.9590E+1	1.418	1.30E-1	1.5200E+2	1.569	1.55E-1
1.8800E+1	1.454	5.50E-4	8.9910E+1	1.434	1.27E-1	1.5249E+2	1.575	1.16E-1
1.9200E+1	1.451	4.35E-4	9.0300E+1	1.451	1.20E-1	1.5300E+2	1.571	8.65E-2
1.9600E+1	1.448	3.60E-4	9.0700E+1	1.464	1.10E-1	1.5357E+2	1.561	6.02E-2
2.0000E+1	1.446	3.05E-4	9.1100E+1	1.474	1.00E-1	1.5432E+2	1.545	3.96E-2
2.0500E+1	1.444	2.52E-4	9.1510E+1	1.482	8.84E-2	1.5520E+2	1.530	2.63E-2
2.1000E+1	1.442	2.12E-4	9.2000E+1	1.487	7.56E-2	1.5618E+2	1.517	1.66E-2
2.1500E+1	1.440	1.83E-4	9.2320E+1	1.490	6.76E-2	1.5700E+2	1.508	1.18E-2
2.2000E+1	1.439	1.60E-4	9.3150E+1	1.490	4.79E-2	1.5812E+2	1.498	8.20E-3
2.2400E+1	1.438	1.52E-4	9.3980E+1	1.486	3.36E-2	1.5900E+2	1.493	5.89E-3
2.2800E+1	1.437	1.49E-4	9.4860E+1	1.480	2.36E-2	1.6000E+2	1.487	3.25E-3
2.3000E+1	1.437	1.45E-4	9.5720E+1	1.474	1.65E-2	1.6100E+2	1.483	
2.3400E+1	1.436	1.36E-4	9.6620E+1	1.469	1.16E-2	1.6150E+2	1.480	
2.3800E+1	1.436	1.31E-4	9.7530E+1	1.464	8.10E-3	1.6200E+2	1.478	
2.4200E+1	1.435	1.29E-4	9.8500E+1	1.460	5.89E-3	1.6250E+2	1.476	
2.4600E+1	1.434	1.41E-4	9.9430E+1	1.456	4.40E-3	1.6300E+2	1.474	
2.5000E+1	1.434	1.60E-4	1.0040E+2	1.453	2.95E-3	1.6400E+2	1.471	
2.6000E+1	1.433		1.0134E+2	1.451	2.10E-3	1.6500E+2	1.468	
2.7000E+1	1.432		1.0200E+2	1.449		1.7000E+2	1.460	
2.8000E+1	1.431		1.0300E+2	1.447		1.7500E+2	1.456	
3.0000E+1	1.430		1.0400E+2	1.445		1.8000E+2	1.452	
3.2000E+1	1.429		1.0500E+2	1.443		1.8500E+2	1.450	
3.4000E+1	1.428		1.0550E+2	1.442		1.9000E+2	1.449	
3.6000E+1	1.428		1.0600E+2	1.441		1.9500E+2	1.447	
3.9000E+1	1.427		1.0800E+2	1.439		2.0000E+2	1.446	
4.2000E+1	1.426		1.1000E+2	1.437		3.0000E+2	1.440	
4.5000E+1	1.425		1.1200E+2	1.435		4.0000E+2	1.438	
4.8000E+1	1.425		1.1400E+2	1.433		6.0000E+2	1.438	
5.1000E+1	1.424		1.1600E+2	1.431		1.0000E+3	1.437	
5.4000E+1	1.423		1.1800E+2	1.430		2.0000E+3	1.437	
5.7000E+1	1.422		1.2000E+2	1.428		1.0000E+4	1.437	
6.0000E+1	1.421		1.2200E+2	1.427		5.0000E+4	1.437	
6.3000E+1	1.420		1.2400E+2	1.425		2.0000E+5	1.438	

that the labels on the ordinates in their Figs. 1 and 2 are too small by a factor of ~ 4 , making the disagreement with Kuan not so large but still serious.

Fink and Sill⁵ obtained preliminary values of m_{Im} at two wavelengths in the 90- μm line at $T = 90$ K. These values (plotted in Fig. 12) are rather higher than those of Kuan adjusted to 100 K.

B. Choice of Imaginary Index

The measurements of Kuan are favored over those of BK because of the internal inconsistency of BK's paper. Kuan's spectral resolution was also better. Kuan found that both peaks shift to lower frequency with increasing temperature, which causes him to disagree with BK not only in intensity of the lines but also in their locations.

It would be desirable to reanalyze the raw transmission data of Kuan at 100 K because m_{Im} is large enough that m_{Re} varies somewhat across the absorption lines. However, the raw data were not included in Kuan's thesis. Our scaling from 4.2 to 100 K is based on changes in peak position, width, and integrated intensity given by Kuan, but there may also be changes in the shapes of the peaks which we cannot know. Kuan's measurements are not reanalyzed here because of this uncertainty in reconstructing the raw data for 100 K and because m_{Re} varies only moderately across these lines (from 1.33 to 1.58, as shown in Sec. VII). Any postulated changes in the strengths of these lines will affect m_{Re} significantly only in the immediate vicinity of the lines, as shown below.

VI. Microwave

Simpson, Fair, and Howard⁴¹ (1980) prepared samples of packed CO_2 snow of varying density in the 0.7–1.27-g cm^{-3} range. They were able to infer properties of pure CO_2 from microwave measurements by assuming that scattering was negligible since the airspaces in their packed snow blocks were much smaller than the wavelengths used, $25 < \lambda < 136$ mm (frequencies 2.2–12 GHz). They extrapolated their measurements to the density of pure CO_2 obtaining $\epsilon_{\text{Re}} = 2.25$ independent of frequency in this range and also independent of temperature between 113 and 183 K. They estimated an uncertainty of 10% in ϵ_{Re} , which gives us $m_{\text{Re}} = 1.5 \pm 0.1$. An upper limit to the loss tangent was obtained, $\tan \delta \equiv \epsilon_{\text{Im}}/\epsilon_{\text{Re}} < 0.005$, implying $m_{\text{Im}} < 0.004$ throughout this frequency range. Some less accurate measurements by the same authors suggested that these results for both m_{Re} and m_{Im} remain valid out to much longer wavelength, at least to $\lambda = 6$ m (frequency 50 MHz).

VII. Kramers-Kronig Analysis

Analysis of the entire spectrum using the Kramers-Kronig relation (1) to obtain a self-consistent set of $m_{\text{Re}}(\lambda)$ and $m_{\text{Im}}(\lambda)$ involves (a) scaling the x-ray or UV band strengths to obtain the correct m_{Re} at visible wavelengths; (b) reanalysis of transmittance data in the strong IR bands using trial values of $m_{\text{Re}}(\lambda)$; and (c)

computation of the entire spectrum of $m_{\text{Re}}(\lambda)$. These three steps are iterated to convergence.

A. Scaling of X-Ray and UV Imaginary Index

The real index of refraction is known at visible wavelengths. When the real index is computed at all wavelengths using Eq. (1), its value in the visible is largely controlled by the strengths of the x-ray and UV absorption bands. The x-ray band is known only in position and shape, not in strength, so we are free to adjust its strength to obtain the correct observed value of m_{Re} in the visible.

The reference value of m_{Re} is taken from measurements of Seiber *et al.*²⁵ shown in Fig. 2: $m_{\text{Re}} = 1.404$ at $\lambda = 1.0 \mu\text{m}$. When the Koch and Skibowski¹⁹ values of m_{Im} are used for the UV, the x-ray band is required to have a huge peak value of $m_{\text{Im}} = 13.7$. Daniels values of m_{Im} in the UV are considerably larger, implying a real index at $1.0 \mu\text{m}$, which is too large even if the x-ray band is completely omitted from the KK analysis. Thus, for the compilation, Daniels values of m_{Im} had to be reduced by 4% to obtain the correct m_{Re} at $1.0 \mu\text{m}$ using no x-ray band.

The real index has also been measured in the microwave region,⁴¹ $m_{\text{Re}} = 1.5 \pm 0.1$. Thus the microwave real index is not significantly different from the visible real index. It is interesting to contrast this situation with the case of water ice, where the real index rises from 1.3 in the visible to 1.8 in the microwave.¹⁵ That rise is due mainly to two far-IR absorption bands. CO_2 ice also has two far-IR bands, but they are so narrow (compared with water-ice bands) that their integrated strength is small. According to our KK calculation, they cause m_{Re} to rise from 1.404 (visible) only up to 1.438 (microwave). The values of m_{Im} in the far IR are uncertain, because to infer them required a temperature correction. If the microwave real index were known accurately, it could be used as a constraint to adjust the strengths of the far-IR lines as was done for water ice. However, the uncertainty of the microwave real index is too large to allow it to be used as a constraint.

B. Analysis of Transmittance Data at 4.3 and 15 μm

To obtain m_{Re} and m_{Im} in the 4.3- and 15- μm bands, the transmission data of Yamada and Person⁷ must be analyzed by the method described in the Appendix. The results of the reanalysis are dramatic. At the 15.1- μm peak, YP's original value of $m_{\text{Im}} = 6.4$ is reduced to $m_{\text{Im}} = 1.8$, and the relative heights of the two peaks in the doublet are reversed (Fig. 8).

C. Computation of Real Index

For use in computation, Eq. (1) is modified to the form used by Warren¹⁵:

$$m_{\text{Re}}(\nu) = 1 + \frac{2}{\pi} P \int_0^\infty \frac{\nu'^2 m_{\text{Im}}(\nu') - \nu \nu' m_{\text{Im}}(\nu)}{\nu'^2 - \nu^2} d \ln \nu', \quad (12)$$

where ν is wave number. This equation is equivalent to Eq. (1) but is more convenient for numerical computations because its singularity is of the 0/0 type. Near-

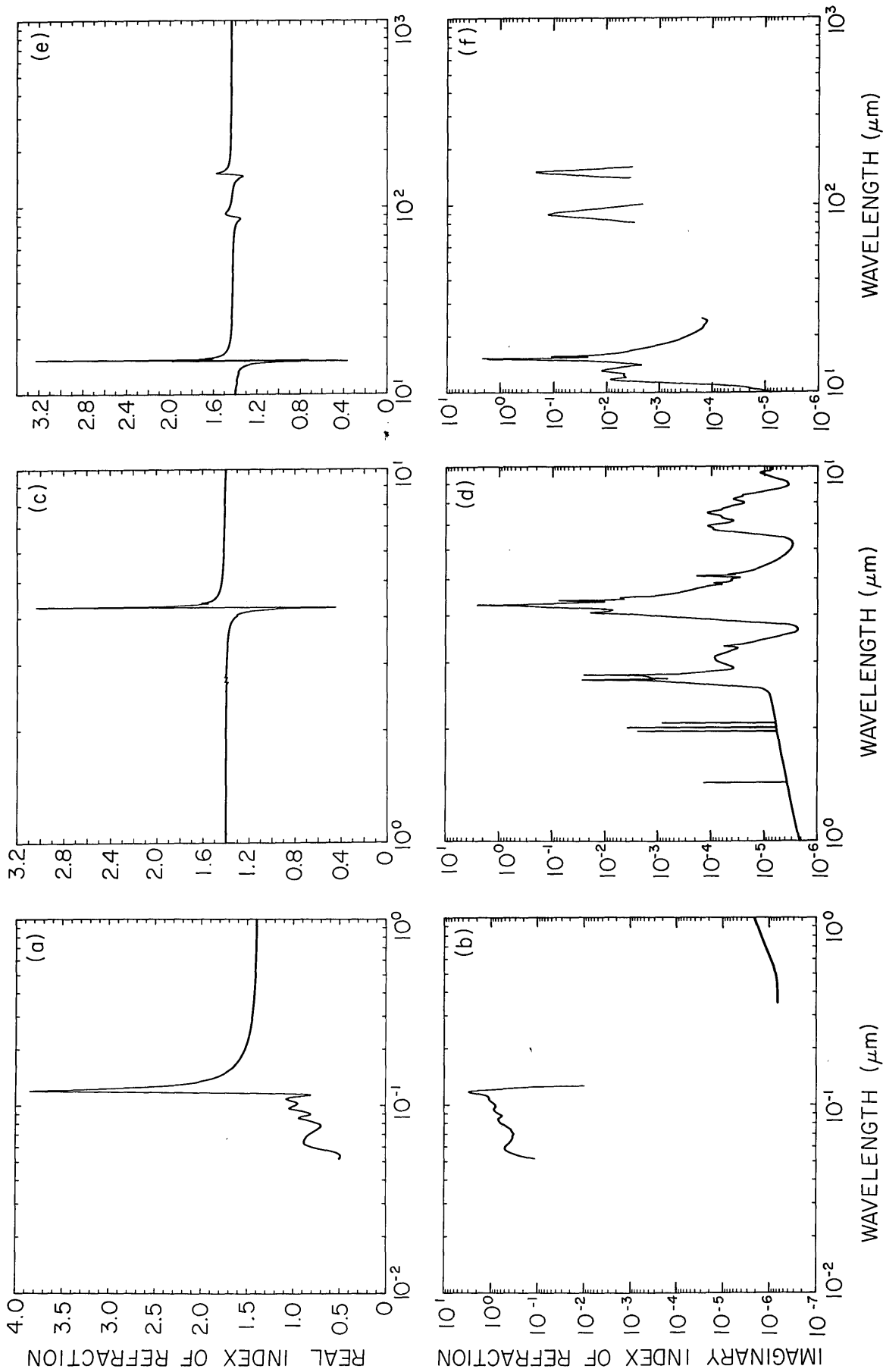


Fig. 14. Compilation of real and imaginary parts of the refractive index of CO_2 ice. Data sources and uncertainties are discussed in the text. These graphs are tabulated in Table I. Details of the strong absorption bands, which cannot be resolved in this figure, are shown as the solid lines in Fig. 15.

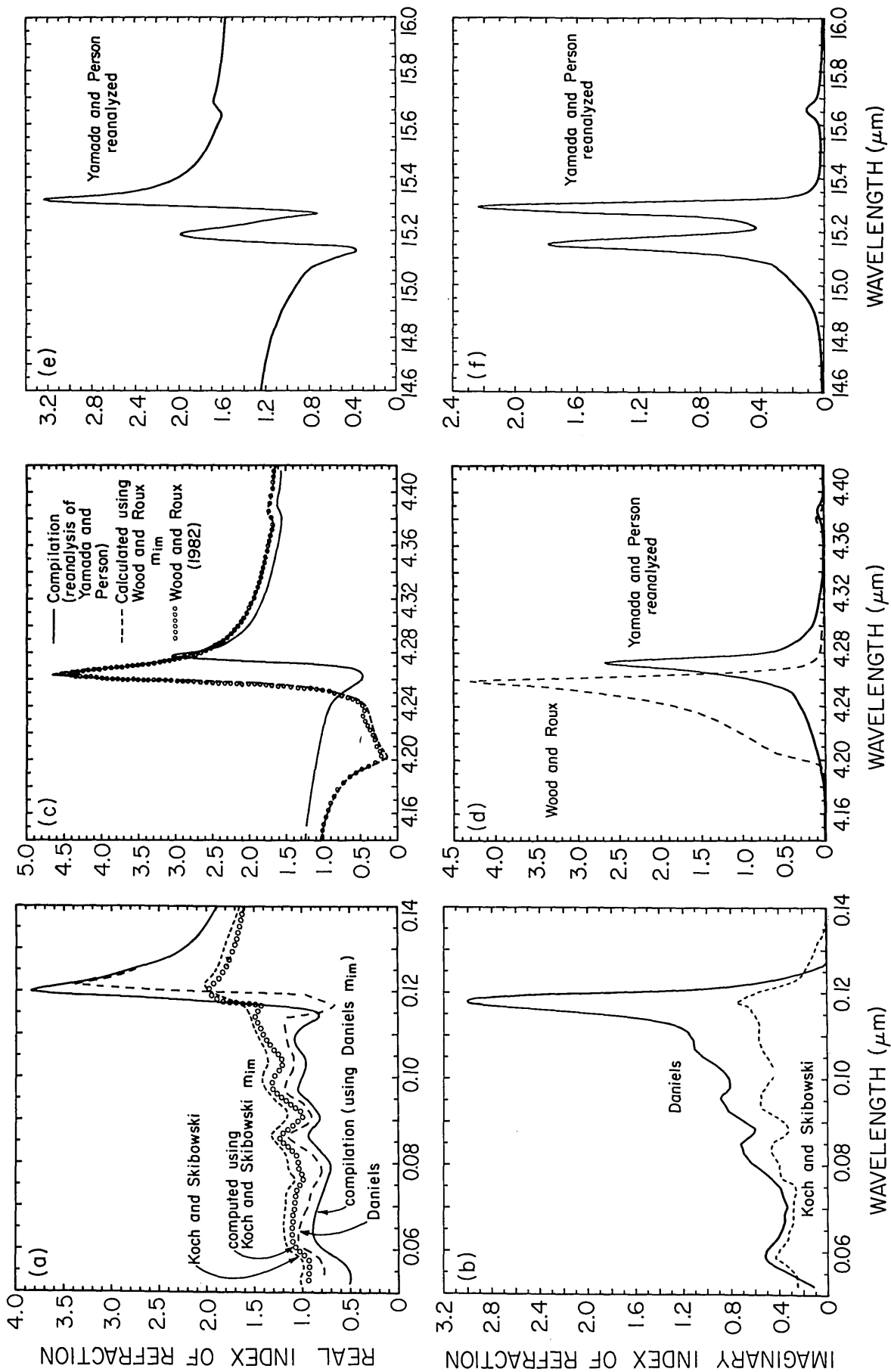


Fig. 15. Details of the strong absorption bands of CO_2 ice. The solid lines give the same values shown in Fig. 14 but are plotted here on an expanded wavelength scale; they are tabulated in Table I. The dashed line in (a) shows that the results of Daniels¹⁷ differ somewhat from the compilation, which applies Kramers-Kronig analysis to the m_{im} of Daniels, as discussed in Sec. VII.C. The short-dash lines in (a) and (b) are an alternative set of refractive-index values, using m_{im} as obtained by Koch and Skibowski¹⁹ (KS) and m_{re} as calculated here from KS's m_{im} using KK analysis. This m_{re} differs somewhat from that obtained by KS (line of circles) as discussed in Sec. VII.C. The dashed lines in (c) and (d) are an alternative set of refractive-index values obtained by applying KK analysis to the m_{im} of Wood and Roux³¹ as discussed in Sec. VII.C; the m_{re} thus obtained agrees well with the m_{re} as reported by Wood and Roux (circles).

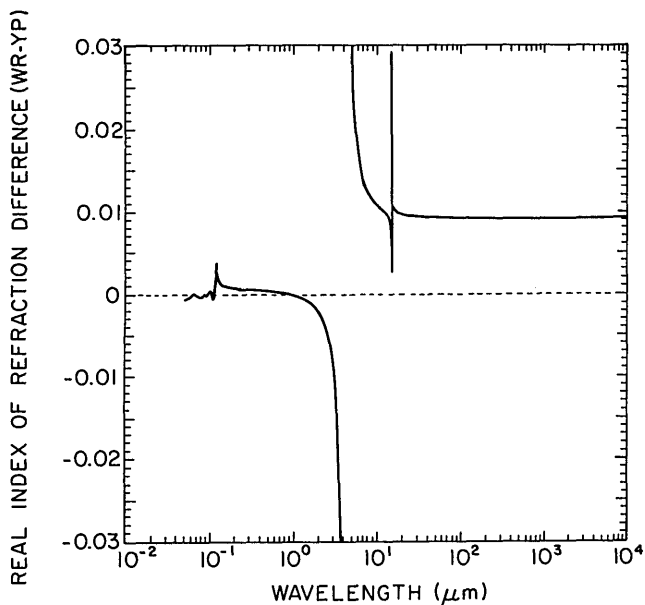


Fig. 16. Solid line shows the difference in $m_{Re}(\lambda)$, outside the 4.3- μm band, obtained in the Kramers-Kronig analysis if the data of Wood and Roux³¹ (WR) are used in place of those of Yamada and Person⁷ (YP) for the 4.3- μm band. The large difference in m_{Re} within the band exceeds the bounds of this figure and is shown in Fig. 15(c).

ly 1000 wavelengths (listed in Table I) are chosen to represent the spectrum. This large number of wavelengths is necessary to resolve adequately the often abrupt variations in both m_{Re} and m_{Im} . The integral in Eq. (12) is evaluated numerically using $\sim 30,000$ quadrature points (32 points between each pair of neighboring wavelengths).

Four independent computations are done: using either Daniels¹⁸ or Koch and Skibowski¹⁹ as the source of UV data and either Yamada and Person⁷ or Wood and Roux³¹ for the 4.3- μm band. The results for the refinement using Daniels and Yamada and Person are shown in Fig. 14 and tabulated in Table I. Details of the strong absorption bands showing results of all four analyses are shown in Fig. 15.

The effect of alternative sources of UV data is to cause large variations in m_{Re} only in the UV; there is no difference beyond 1.0 μm because m_{Re} is fixed at that point in both refinements. Differences in the visible are smaller than 0.02: at $\lambda = 0.3 \mu\text{m}$, $m_{Re} = 1.427$ if KS's data are used, and $m_{Re} = 1.448$ if Daniels data are used. The UV values from both refinements are shown in Figs. 15 (a) and (b) so that if future evidence disputes our choice of Daniels data for the compilation, the alternative values can be read off the figure.

The Daniels $m_{Im}(\lambda)$, reduced by 4% to match the visible real index as discussed above, was used to compute UV values of $m_{Re}(\lambda)$, shown as the solid line in Fig. 15(a). These m_{Re} do not agree with the values of m_{Re} obtained from the Daniels paper [dashed line in Fig. 15(a)]. This difference is probably due mainly to the difficulty of reading values of wavelength accurately from Daniels' separate plots of ϵ_{Re} and ϵ_{Im} in the small

published graphs. The values of m_{Re} computed here using the $m_{Im}(\lambda)$ of KS also do not agree with the values obtained by KS (Koch; personal communication), as is also shown in Fig. 15(a). In this case the discrepancy is probably due to different assumptions about the behavior of m_{Im} outside the region measured.

Figures 15(c) and (d) show the results of refinements using alternative sources of data for the 4.3- μm band. Also plotted is $m_{Re}(\lambda)$ as given by Roux *et al.*,³⁴ showing that our KK analysis is in excellent agreement with theirs. The slight differences between 4.20 and 4.24 μm are probably due to the smoothing of WR's $m_{Im}(\lambda)$, which was done in this work.

The compilation uses YP for the 4.3- μm band. The effect of using WR instead is to cause large changes in m_{Re} only close to the band [Fig. 15(c)]; the much smaller changes at other wavelengths are given in Fig. 16. The greater strength of the 4.3- μm band in WR's data causes m_{Re} to be larger by 0.01 in the limit of long wavelength. Through the effect of m_{Re} on reflectivity, this also causes larger variations in m_{Re} of up to 0.03 at 15 μm when the transmittance data of YP are analyzed. The values of m_{Im} at 15 μm change by at most 0.0015 (at the peak at 15.155 μm) if WR is used instead of YP at 4.3 μm .

If future evidence supports the use of WR's data at 4.3 μm , the values in the table can be replaced by reading values from Figs. 15(c) and (d) and 16.

There are gaps in the imaginary index plots in Fig. 14 where no information is available. These same regions are also left blank in Table I. The 1.0–2.5- μm region also lacks measurements (except in the four narrow lines); here the compilation of m_{Im} is just the result of a long interpolation. There are three other regions where small values of m_{Im} are highly uncertain: near 3.6, 6, and 9 μm . They were obtained from reanalysis of DK's transmittance data as described in Sec. IV.B. The correct values of m_{Im} in these three regions may be as much as a factor of 10 larger than the stated values or many orders of magnitude smaller. (We have no constraint on a lower limit from this experiment.) The values in the table are marked with double asterisks to indicate this.

The number of significant digits included in the table is not an indication of the accuracy of the optical constants. The real index is known no better than ± 0.05 , but differences in real index from one wavelength to another are known much more accurately, and three decimal places are needed to resolve these differences. The uncertainty in spectral location of the absorption peaks is also considerable in many cases, but wavelength differences within an absorption band are sometimes much more accurately known. To resolve the variation of m_{Im} with wavelength within the near-IR line at 1.4 μm (Fig. 5), six significant figures were needed for wavelength, but the actual location of the line is far less certain.

As this paper has emphasized, there is much work needed on measurement of the optical constants of CO₂ ice. The table is, therefore, not a definitive set of

optical constants but is offered for use until better measurements are available.

VIII. Summary and Recommendation for Needed Measurements

A compilation of the complex refractive index of CO₂ ice is made from the UV to the far-IR with some gaps. The uncertainty of this compilation varies greatly with wavelength and can be judged by noting in the figures the discrepancy among measurements by different investigators. The imaginary index is probably accurate to $\pm 20\%$ from 0.3 to 1.0 μm and from 6.6 to 8.6 μm . In the UV and in the strong bands the uncertainty of both m_{Im} and m_{Re} is a factor of ~ 2 . In the IR, outside the strong bands, the uncertainty is a factor of ~ 5 except in the regions noted in the table near 3.6, 6, and 9 μm , where the uncertainty is more than a factor of 10. Alternative compilations are provided for the UV and the 4.3- μm band, where it is not clear which of two conflicting sets of data is best.

The real index by contrast can be stated rather more accurately. Although the absorption bands at 4.3, 15, 90, and 150 μm have large peak values, their integrated strengths are too small to have much effect on m_{Re} at wavelengths far from the absorption maxima. Figures 14(a), (c), and (e) show that the value of m_{Re} away from the absorption bands varies only in the range from 1.40 (at 1 μm) to 1.44 (microwave) for $T > 77$ K. The uncertainty is about ± 0.05 , judging from Fig. 2.

New measurements are needed in several spectral regions. The first priority is to measure the weakly absorbing regions of the IR, 1–25 μm . Except for the 6.5–8.5- μm region, which is known accurately, the IR studies used CO₂-ice samples which scattered a substantial but undetermined amount of light. A second priority is to remeasure the near-UV and visible absorption, 0.2–1.0 μm . The reported values are likely to be correct, but because the measurements were made on impure CO₂ they require confirmation. Samples at least several millimeters thick are required for both of these spectral regions; thus the Behn-Gaizauskas method for growing large clear crystals of pure CO₂ should be revived.

A third priority is to obtain additional measurements in the UV and in the strong IR bands. These regions have already been studied by several authors, but there is considerable discrepancy among the derived values. Attempts should be made to obtain smooth plane surfaces of CO₂-ice crystals, so that reflection measurements can be made in addition to the transmission measurements which have been used up to now.

Finally, we note that it has been useful to reinterpret here the raw data from some of the experiments where it was possible to improve on the original interpretation. In order that data can remain useful for such attempts at reinterpretation, it is important that not just the derived quantities but also the raw data always be published, preferably in graphs of large size.

I thank Richard Dittion and Willis Person for providing large graphs of their IR transmittance data, E.

E. Koch for providing unpublished values of ultraviolet optical constants, Uwe Fink and J. A. Roux for providing tables of their infrared optical constants, and the above authors as well as Walter Egan, Victor Gaizauskas, and T. S. Kuan for helpful discussion. This work was supported by NSF grant ATM-82-15337. The computations were done at the National Center for Atmospheric Research.

Appendix. Analysis of Transmittance Data at 4.3 and 15 μm

The experimental arrangement of Yamada and Person⁷ (YP) involved three layers (air–window–air) for the blank compared with four layers (air–CO₂–window–air) for the sample. Other parts of the apparatus were identical in the two cases. AgCl and CsBr windows were used, respectively, for the 4.3- and 15- μm measurements (YP's Table II). The refractive indices are $m_{\text{Re}} = 1.98$ for AgCl and 1.64 for CsBr (Ref. 38) and $m_{\text{Re}} = 1.4$ for CO₂ outside the absorption bands. The interface reflectivities outside the bands then are 0.059 for CsBr–air, 0.006 for CsBr–CO₂, 0.028 for CO₂–air, 0.108 for AgCl–air, and 0.029 for AgCl–CO₂. The system reflectivity outside the bands (including multiple reflections) is then $R_0(\lambda_{\text{out}}) = 0.195$ for the blank and $R(\lambda_{\text{out}}) = 0.152$ with the sample using the AgCl window. For the CsBr window, $R_0(\lambda_{\text{out}}) = 0.111$ and $R(\lambda_{\text{out}}) = 0.089$.

As a starting point for the analysis we need the true transmittance through the sample $t(\lambda)$. What was plotted by YP, however, was $\log(t_0/t)$, where t_0 is the transmittance of the blank after subtracting a background based on measurements outside the band. However, a partial background remains in their figures. We first subtract the remaining background, so that now the entire original background, $\log[t_0/t(\lambda_{\text{out}})]$, has been subtracted, where λ_{out} is a wavelength outside the band. We thus now have plotted $\log[t_0/t(\lambda)] - \log[t_0/t(\lambda_{\text{out}})]$, which is the same as $\log[t(\lambda_{\text{out}})] - \log[t(\lambda)]$. So now, by adding

$$-\log[t(\lambda_{\text{out}})] = -\log[1 - R(\lambda_{\text{out}})] = \begin{cases} 0.072 \text{ for AgCl window} \\ 0.040 \text{ for CsBr window} \end{cases},$$

we obtain the value of $-\log_{10}(t(\lambda))$.

An iterative procedure is then followed to find the spectrum $[m_{\text{Re}}(\lambda), m_{\text{Im}}(\lambda)]$, which is consistent with Kramers-Kronig relations and also with the observed transmission data: We start with a trial spectrum of $m_{\text{Im}}(\lambda)$ and compute $m_{\text{Re}}(\lambda)$ using Eq. (1). Then we calculate the system reflectivity $R(\lambda)$ at each wavelength in the 4.3- and 15- μm bands. This, together with the observed $t(\lambda)$, implies $m_{\text{Im}}(\lambda)$, as described in the following paragraph. Then the new calculated $m_{\text{Im}}(\lambda)$ is used together with the rest of the spectrum to recompute $m_{\text{Re}}(\lambda)$. The two steps, (a) computation of $m_{\text{Re}}(\lambda)$ from $m_{\text{Im}}(\lambda)$ using KK analysis and (b) computation of $m_{\text{Im}}(\lambda)$ in the bands using $m_{\text{Re}}(\lambda)$ and $t(\lambda)$, are iterated to convergence. In practice, it is necessary to damp both steps of this refinement procedure in order to avoid oscillations.

The computation of $m_{\text{Im}}(\lambda)$, given $m_{\text{Re}}(\lambda)$ and $t(\lambda)$, proceeds as follows. Define R_1 , R_2 , and R_3 to be the

reflectivity of air—window, CO₂—window, and CO₂—air interfaces, respectively. Then at a particular wavelength, the transmittance reduced solely by reflection in one pass is

$$t_R = (1 - R_3)(1 - R_2)(1 - R_1), \quad (8)$$

and the transmittance reduced solely by absorption in one pass is

$$t_A = \exp(-k_{\text{abs}}d), \quad (9)$$

where d is the sample thickness measured by YP. Then the system transmittance is given by

$$t = \frac{t_R t_A}{1 - R_1 R_2} + \frac{t_R t_A^3}{1 - R_1 R_2} [R_2 R_3 + R_1 R_3 (1 - R_2)^2]. \quad (10)$$

This accounts for all possible multiple reflections within the nonabsorbing window and accounts for up to three passes through the CO₂ film due to multiple reflections, which is sufficient even if absorption is negligible. In fact, the second term in Eq. (10) is negligible at all wavelengths in the absorption band to which this analysis is applied; so we obtain t_A using only the first term:

$$t_A = (1 - R_1 R_2)t/t_R. \quad (11)$$

Then Eq. (9) is used to obtain k_{abs} and thus m_{Im} .

The samples used by YP had a thickness of less than one wavelength, so the theory of thin-film transmittance is applicable. However, that theory [Eqs. (2) and (3) of the Appendix of Sill *et al.*³²] reduces to our simpler formula Eq. (11) for the case of large absorption, which is valid for all wavelengths to which this procedure is applied.

References

- J. B. Pollack and O. B. Toon, "Quasi-Periodic Climate Changes on Mars: A Review," *Icarus* **50**, 259 (1982).
- L. G. Liu, "Dry Ice II, a New Polymorph of CO₂," *Nature London* **303**, 508 (1983).
- R. W. G. Wyckoff, *Crystal Structures, Vol. 1* (Wiley, New York, 1963), p. 368.
- N. H. Hartshorne and A. Stuart, *Crystals and the Polarizing Microscope* (Edward Arnold, London, 1970), p. 19.
- U. Fink and G. T. Sill, "The Infrared Spectral Properties of Frozen Volatiles," in *Comets*, L. L. Wilkening, Ed. (U. of Arizona Press, Tucson, 1982), pp. 164–202.
- S. G. Warren and W. J. Wiscombe, "Spectral Albedo and Emisivity of CO₂-Frost in Martian Polar Caps: Model Results," *Icarus* (submitted).
- H. Yamada and W. B. Person, "Absolute Infrared Intensities of the Fundamental Absorption Bands in Solid CO₂ and N₂O," *J. Chem. Phys.* **41**, 2478 (1964).
- K. M. Monahan and W. C. Walker, "Photoabsorption of Solid Carbon Dioxide from 7 to 12 eV," *J. Chem. Phys.* **61**, 3886 (1974).
- W. G. Egan and F. A. Spagnolo, "Complex Index of Refraction of Bulk Solid Carbon Dioxide," *Appl. Opt.* **8**, 2359 (1969).
- U. Behn, "Ueber die Dichte der Kohlenäure im festen und flüssigen Zustande," *Ann. Phys.* **308**, 733 (1900).
- V. Gaizauskas, "Studies of the Infrared and Raman Spectra of Gaseous, Liquid and Solid Carbon Dioxide," Ph.D. Thesis, U Toronto, Canada (1955).
- R. A. Blest-Castillo, "Infrared Absorption of Solid Carbon Dioxide in the Frequency Range 1100 cm⁻¹-1600 cm⁻¹," M.S. Thesis, U. Toronto, Canada (1970).
- L. Mannik and E. J. Allin, "The ($\nu_1, 2\nu_2$) Vibron-Phonon Infrared Absorption Band of Solid CO₂," *Can. J. Phys.* **50**, 2105 (1972).
- R. Dittion and H. H. Kieffer, "Optical Properties of Solid CO₂: Application to Mars," *J. Geophys. Res.* **84**, 8294 (1979).
- S. G. Warren, "Optical Constants of Ice from the Ultraviolet to the Microwave," *Appl. Opt.* **23**, 1206 (1984).
- A. S. Koster, "Oxygen K Emission Spectra of Ice, Solid Carbon Dioxide, and Solid Alcohols," *Appl. Phys. Lett.* **18**, 170 (1971).
- J. Daniels, "Optical Constants of the Solid Atmospheric Gases N₂, O₂ and CO₂," *Opt. Commun.* **2**, 352 (1970).
- J. Daniels, C. v. Festenberg, H. Raether, and K. Zeppenfeld, "Optical Constants of Solids by Electron Spectroscopy," in *Springer Tracts in Modern Physics, Vol. 54* (Springer-Verlag, Heidelberg, 1970), p. 78.
- E. E. Koch and M. Skibowski, "Electronic Excitation of Solid Carbon Dioxide in the Extreme Ultraviolet," *Chem. Phys. Lett.* **14**, 37 (1972).
- M. Born and E. Wolf, *Principles of Optics* (Pergamon, Oxford, 1975), pp. 628–629.
- G. Andermann, A. Caron, and D. A. Dows, "Kramers-Kronig Dispersion Analysis of Infrared Reflectance Bands," *J. Opt. Soc. Am.* **55**, 1210 (1965).
- F. Stern, "Elementary Theory of the Optical Properties of Solids," in *Solid State Physics, Vol. 15* (Academic, New York, 1963), p. 300.
- J. H. Fock, H. J. Lau, and E. E. Koch, "Electronic Band Structure of Solid CO₂ as Determined from the $h\nu$ -Dependence of Photoelectron Emission," *Chem. Phys.* **83**, 377 (1984).
- K. M. Monahan and W. C. Walker, "Vacuum Ultraviolet Absorption Spectra of Solid N₂O and CO₂ at 53K," *J. Chem. Phys.* **63**, 1676 (1975).
- B. A. Seiber, A. M. Smith, B. E. Wood, and P. R. Müller, "Refractive Indices and Densities of H₂O and CO₂ Films Condensed on Cryogenic Surfaces," *Appl. Opt.* **10**, 2086 (1971).
- R. S. Nakata, K. Watanabe, and F. M. Matsunaga, "Absorption and Photoionization Coefficients of CO₂ in the Region 580–1670 Å," *Sci. Light* **14**, 54 (1965).
- H. Abe and R. Onaka, "Molecular Excitons of Solid Carbon Dioxide," *J. Phys. Soc. Jpn.* **53**, 1176 (1984).
- K. E. Tempelmeyer and D. W. Mills, Jr., "Refractive Index of Carbon Dioxide Cryodeposit," *J. Appl. Phys.* **39**, 2968 (1968).
- J. Kruger and W. J. Ambis, "Optical Measurements on Thin Films of Condensed Gases at Low Temperatures," *J. Opt. Soc. Am.* **49**, 1195 (1959).
- W. Schulze and H. Abe, "Density, Refractive Index and Sorption Capacity of Solid CO₂ Layers," *Chem. Phys.* **52**, 381 (1980).
- B. E. Wood and J. A. Roux, "Infrared Optical Properties of Thin H₂O, NH₃, and CO₂ Cryofilms," *J. Opt. Soc. Am.* **72**, 720 (1982).
- G. Sill, U. Fink, and J. R. Ferraro, "Absorption Coefficients of Solid NH₃ from 50 to 7000 cm⁻¹," *J. Opt. Soc. Am.* **70**, 724 (1980).
- H. Yamada and W. B. Person, "Absolute Infrared Intensities of the Fundamental Absorption Bands in Solid CS₂," *J. Chem. Phys.* **40**, 309 (1964).
- J. A. Roux, B. E. Wood, and A. M. Smith, "IR Optical Properties of Thin H₂O, NH₃, and CO₂ Cryofilms," Arnold Engineering Development Center Tech. Rep. AEDC-TR-79-57 (1979); NTIS accession number AD-A074913.
- D. A. Dows and V. Schettino, "Two-Phonon Infrared Absorption Spectra in Crystalline Carbon Dioxide," *J. Chem. Phys.* **58**, 5009 (1973).
- J. T. Houghton, *The Physics of Atmospheres* (Cambridge U.P., Cambridge, 1977).
- M. E. Jacox and D. E. Milligan, "The Infrared Spectra of Thick Films of CO₂ and CO₂ + H₂O at Low Temperatures," *Spectrochim. Acta* **17**, 1196 (1961).
- W. L. Wolfe, *Handbook of Military Infrared Technology* (U.S. GPO, Washington, D.C., 1965).

39. T. S. Kuan, "I. Lattice Vibrations of Solid α -Nitrogen and Atom-Atom Intermolecular Potential. II. Intensities of the Far-Infrared Absorption Lines of Solid Carbon Dioxide," Ph.D. Thesis, U. Southern California, Los Angeles (1969).
40. K. G. Brown and W. T. King, "Infrared Intensities of the Lattice Modes of Solid Carbon Dioxide," J. Chem. Phys. 52, 4437 (1970).
41. R. A. Simpson, B. C. Fair, and H. T. Howard, "Microwave Properties of Solid CO_2 ," J. Geophys. Res. 85, 5481 (1980).

Patter continued from page 2634

Detector arrays with image-plane processing

Previous approaches to machine vision have concentrated on special-purpose computational hardware, including focal-plane processor chip technologies. In most cases, detection and processing are considered as distinct submodules. In a newly proposed device, edge processing of picture elements is incorporated on the same VLSI (very-large-scale integration) chip as that of the image-detection elements.

The concept combines relatively large detector elements with small processor elements as VLSI chip features and can have many specific embodiments. Previous VLSI and VHSIC (very-high-speed integrated circuit) processor-chip designs have generally sought to diminish all individual features on the chip to the smallest size possible and have not merged detection with processing. The new device concept retains relatively large detector element sizes (perhaps 10 to 100 μm or larger in diameter) with processing-electronics components of much smaller size (2 μm or less), filling in gaps left between the detector-element active areas.

The specific design concept shown schematically in Fig. 8 is for realizing a difference-of-Gaussian (DOG) operator in a detector/processor array for use in machine-vision edge-enhancement and edge-detection applications. A sequential approach to input voltages and readout is shown, but a parallel approach is also possible if readout and voltage distribution points feed through to the base of the substrate material.

The principal functional components for creating a DOG operator are the inversion and attenuation of the signals from the six detector elements surrounding the central element and the summation of various signal contribu-

tions for readout. The attenuation factor is about one-sixth for the six surrounding elements. A lens-blur function smooths the detector-element spatial response to obtain approximately a DOG-group response function and minimizes the effect of gaps between adjacent detector elements.

This work was done by Daniel J. Jobson of Langley Research Center. Refer to LAR-13391. Further information may be found in NASA TM-85809 [N84-25927], "Edge Analyzing of Center/Surround Response Functions in Cybernetic Vision" [\$8.50]. A copy may be purchased [prepayment required] from NITS.

Integrated-circuit active digital filter

New digital integrated-circuit chips with pipeline architecture rapidly move 35×35 2-D convolutions. There is a need for such circuits in image enhancement, data filtering, correlation, pattern extraction, and synthetic-aperture-radar image processing, all of which require repeated calculations of weighted

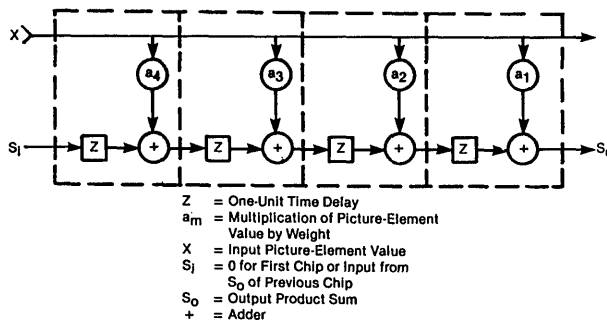


Fig. 9. Picture-element values and partial sums flow through delay-adder modules like this one. After each cycle or time unit of the calculation, each value in the filter moves one position to the right.

sums of values from images or 2-D arrays of data.

A set of chips (each containing a one-by-five set of multiplier/adders) can serve as a fast digital filter when attached to a host computer. In an $m \times n$ digital filter, for example, processing an image of 1000×1000 elements, each element value is replaced by a weighted sum of the values of an $m \times n$ rectangular subarray of elements centered on the given element. For this new hardware, each value and each weight are fetched from memory only once. First the $m \times n$ array of weights is loaded into the filter, where it remains throughout the calculation. Then the image data are shifted into and through the filter as the filtered element values are calculated. A general-purpose computer would perform the same calculation much more slowly: Each element value would be fetched from memory $m \times n$ times, once for each element of the weighting subarray in which it appears.

Each chip contains five multiplier/adders executed in metal-oxide semiconductor circuitry. A delay-adder modular design (see Fig. 9) provides a bucket-brigade transfer of the accumulated product sum, thereby saving multiple accesses to the host computer memory. As many of these chips as necessary can be cascaded together to form an array containing $m \times n$ multipliers. Delay lines are used to retain data between use in succeeding rows of the filter. For example, one row of a 35×35 filter would require seven chips. The chips for one such row will fit in one 68-pin flatpack 90 by 40 mm in dimension.

Both the data and the sums move through the chip in a pipelined manner. Each of the 1225 multiplications and additions taking place at any given moment contributes to a different weighted sum.

This work was done by Robert Nathan of Caltech for NASA's Jet Propulsion Laboratory. Refer to NPO-16020.

Deformable subreflector computed by geometric optics

SUBFORMING employs geometric optics in determining subreflector coordinates to match a main reflector surface with known distortions. An antenna with a distorted paraboloidal reflecting surface can be forced to produce a uniform wave front by using a Cassegrainian geometry with a path-length-compensating subreflector.

First, the computed distortion vectors of the main reflector are best fitted to a paraboloid. Second, the resulting residual distortion errors are used to determine a compensating subreflector surface by ray tracing, using geometric optics. The solution is a set of points defining the subreflector contour. The slope of the surface and the normal to the surface are determined for each point.

This program is written in FORTRAN V for batch execution and has been implemented on a Univac 1100-series computer with a memory requirement of approximately 25K of 36-bit words. The SUBFORMING program was developed in 1983.

This program was written by William F. Williams of Caltech for NASA's Jet Propulsion Laboratory. Refer to NPO-16405.

continued on page 2777

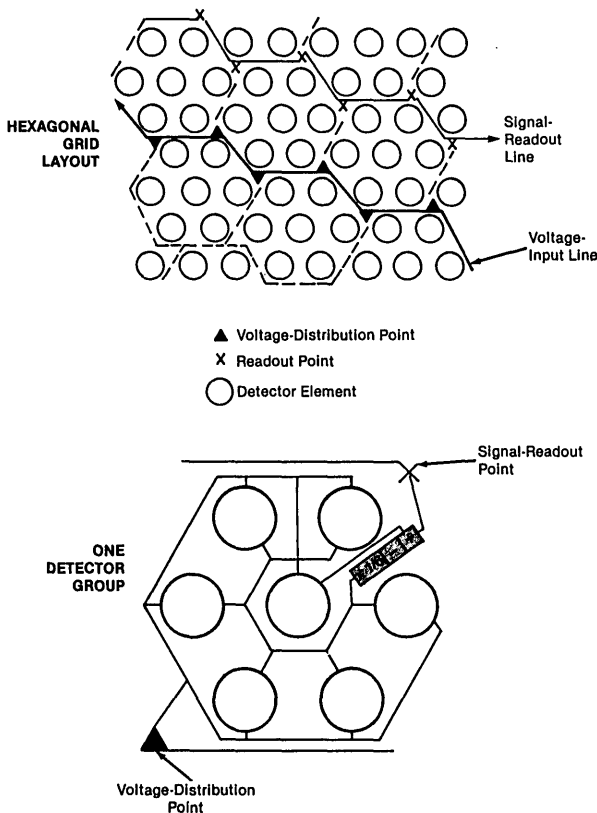


Fig. 8. Detector-array device would help to perform the difference-of-Gaussian operation for use in machine-vision edge enhancement and edge detection.